forests

MDPI

Article

Assessing Community and Protected Area Exposure to Wildfires in Navarra, Spain

Fermín Alcasena [1,*], Alan Ager [2], Julia Loján [1], Isabel Pinto [1], Ignacio García [3], Pere Gelabert [4], Mikel Repáraz [5] and Cristóbal Molina [5]

[1] Institute for Sustainability & Food Chain Innovation (IS-FOOD), Department of Engineering, Public University of Navarre, Arrosadia Campus, 31006 Pamplona, Spain; julia.lojan@unavarra.es (J.L.); catalina.pinto@unavarra.es (I.P.)
[2] USDA Forest Service, Rocky Mountain Research Station, Missoula Fire Sciences Laboratory, 5775 US Highway 10W, Missoula, MT 59808, USA; alan.ager@oregonstate.edu
[3] Institute of Smart Cities (ISC), Department of Engineering, Public University of Navarre, Arrosadia Campus, 31006 Pamplona, Spain; ignacio.garcia@unavarra.es
[4] Department of Agriculture and Forest Engineering, University of Lleida, Alcalde Rovira Roure 191, 25198 Lleida, Spain; perejoan.gelabert@udl.cat
[5] Servicio Forestal y Gestión Cinegética, Departamento de Desarrollo Rural y Medio Ambiente, Gobierno de Navarra, C/González Tablas n°9, 31005 Pamplona, Spain; mreparac@navarra.es (M.R.); cristobal.molina.terren@navarra.es (C.M.)
* Correspondence: fermin.alcasena@unavarra.es

Abstract

The unprecedented 2022 wildfire season in Navarra, northern Spain, marked a turning point in regional wildfire management, when seven simultaneous large fires during a June heatwave burned more than 17,000 ha in just a few days, overwhelming suppression capacity and highlighting the limits of a strategy based primarily on ignition prevention and fire suppression. In this study, we implemented a stochastic wildfire modeling system based on the Minimum Travel Time algorithm, historical ignition patterns, spatial fuel data, and spatiotemporal weather variability to assess community and protected area exposure to wildfire. We simulated more than 50,000 fire season replicates under extreme fire weather conditions, estimating annual burn probability across fire intensity classes at 50 m spatial resolution. We then intersected modeled fire perimeters with building footprints representing residential and industrial structures, as well as protected areas, to assess the spatial distribution of exposure across the region. Results showed strong concentration of community exposure, with three fourths of residential and industrial exposure concentrated in just over one third of the total municipal area. Across Navarra, mean annual modeled exposure summed to 120 residential buildings and 16 industrial structures. Across the protected area network, mean annual burned area summed to 90 ha year^{-1}, including 68 ha year^{-1} at flame lengths greater than 2.5 m, while burned forest area was 16 ha year^{-1}. Protected areas in southern Navarra and forested protected areas in central and northern Navarra showed the highest modeled exposure, identifying priority landscapes where prevention, restoration, and evaluation of managed fire options could support more resilient ecosystems. This study provides a scientific basis for improving wildfire risk governance and strengthening the resilience of communities and protected areas under increasing wildfire pressure in the region.

Keywords: wildfire risk; fire modeling; extreme wildfires; protected areas; communities; fuel management

Academic Editor: Viacheslav I. Kharuk

Received: 30 March 2026
Revised: 8 June 2026
Accepted: 13 June 2026
Published: 15 June 2026

1. Introduction

Wildfire activity in southern Europe has heightened concern over the exposure of human and ecological assets to large, high-severity fire events [1–3]. Across Europe, a relatively small proportion of fires accounts for most of the total area burned, and Spain is among the countries most affected by large wildfires [4–6]. In Navarra, this pattern became especially evident during the 2022 fire season, when a June heatwave coincided with seven simultaneous large wildfires that burned more than 17,000 ha within a few days. The event overwhelmed regional suppression and emergency response capacity. Of the 20 fires from Navarra notified to the National Emergency Center in 2022, 19 required state resources, and 4 of the largest June fires required deployment of the Military Emergency Unit [7]. The same episode led to the evacuation of at least 2590 people. Together, these impacts exposed the limitations of a wildfire management strategy centered primarily on ignition prevention and fire suppression. In this sense, the 2022 season marked a turning point for wildfire management in Navarra by underscoring the need to complement suppression capacity with landscape-scale prevention, strategic fuel management, and community adaptation to future extreme wildfire events.

The increasing likelihood of extreme wildfire in Mediterranean regions of southern Europe is linked to both climatic and landscape drivers [8,9]. Prolonged drought, low fuel moisture, and strong wind events create favorable conditions for rapid fire growth, long-distance spread, crown fire activity, and spotting [10,11]. At the same time, rural depopulation, reduced grazing, agricultural abandonment, limited forest management, and long-term fire exclusion have increased fuel loads and both horizontal and vertical fuel continuity across much of the landscape [12,13]. As a result, former agricultural and pastoral mosaics that once constrained fire spread have progressively transitioned toward more continuous and hazardous fuel configurations [14,15]. Although open valleys and southern agricultural plains remain actively managed, including widespread conversion to irrigated agriculture, foothills and mountain slopes have experienced substantial fuel accumulation associated with the abandonment of marginal agricultural lands [16,17]. Together, these changes favor a fire regime increasingly driven by extreme weather, with a greater likelihood of large wildfires that exceed suppression capacity, spread over long distances, and increase exposure of communities and protected areas [18–20].

Reducing the impacts of extreme wildfire requires a shift from reactive emergency response to proactive risk management [21]. Current wildfire science emphasizes three complementary strategies: creating fire-resilient landscapes, fostering fire-adapted communities, and maintaining safe and effective suppression operations [22–24]. Within this framework, fuel treatments in strategic locations and around populated areas are a primary measure for moderating wildfire spread and reducing extreme fire behavior [25–27]. However, preventive resources are limited, and treatments must be prioritized where they are most likely to reduce exposure of valued resources and assets [28–31]. In practice, regional fuel treatment programs often emphasize treatment prescriptions and implementation costs while giving less attention to the need to aggregate treatments at sufficient scale and intensity in high-priority areas to effectively reduce risk. Addressing this challenge requires spatially explicit information on where large wildfires are most likely to occur, how they are likely to spread under adverse fire weather conditions, and which communities and protected areas are most exposed [32].

Stochastic wildfire simulation provides an effective framework for predicting spatial patterns of wildfire likelihood, intensity, and exposure [33–37]. Fire spread models have been widely used to estimate burn probability, characterize expected fire behavior, and evaluate wildfire exposure across large landscapes [38–40]. By integrating ignition probability, fuels, topography, and representative fire weather scenarios, these models generate

large numbers of plausible fire events and support probabilistic inference on wildfire likelihood and intensity [41,42]. In operational settings, simulation outputs can be used to identify areas where fire behavior is likely to exceed suppression capacity, evaluate the spatial effectiveness of fuel treatments, and prioritize mitigation actions for communities and ecological resources [43,44]. This approach is particularly relevant in Mediterranean regions, where most ignitions are human-caused and fire regimes vary strongly along climatic and topographic gradients [45–49].

In this study, we implemented a regional stochastic wildfire modeling system for Navarra to assess exposure of communities and protected areas to large wildfires under representative extreme fire weather conditions. Despite the need for regional-scale probabilistic assessments that capture potential fire spread and fire intensity patterns, no previous study has addressed wildfire exposure at this scale in Navarra. Earlier applications of stochastic wildfire modeling in the region have been limited to smaller study areas [50,51]. Specifically, we combined historical ignition patterns, spatial fuel and canopy data, topography, and pyrome-specific weather scenarios within a batch fire spread modeling framework to estimate annual burn probability across fire intensity classes at fine spatial resolution. We then intersected simulated fire footprints with residential and industrial structures, forested areas, and protected area designations to identify spatial patterns of exposure across the region. The objectives of this study were to (*i*) estimate the regional distribution of annual burn probability and high-intensity fire potential; (*ii*) characterize exposure of community assets and forested areas to simulated wildfire; and (*iii*) evaluate exposure of protected areas and their forested lands across Navarra. Finally, we discuss how these results can inform ongoing risk mitigation programs and help identify priority areas where prevention and mitigation efforts may provide the greatest benefit for wildfire risk governance in Navarra.

2. Materials and Methods

2.1. Study Area

The study area comprises Navarra, located in northern Spain (Figure 1). Navarra spans a pronounced environmental gradient over a relatively small area of 10,391 km^2, from the Pyrenean mountains in the north and northeast to the Ebro basin in the south. Climate conditions range from oceanic in the north to Mediterranean and semi-arid in the south, with mountain conditions occurring in the Pyrenean sectors along the border with France. Elevation and topography vary substantially across the region, creating strong spatial contrasts in vegetation, fuel structure, and potential fire behavior. As a result, Navarra includes a broad range of land covers and fuel types, from humid forested landscapes in the north to drier agricultural and shrub-dominated areas in the south. These environmental gradients are mirrored by marked variation in settlement patterns.

Main urban centers, including Pamplona and its metropolitan area, together with Tudela, Estella, and Tafalla, collectively account for more than 60% of the population of Navarra. Outside of this urban core, settlement patterns are more dispersed, with small rural communities predominating in the northern and northwestern pre-Pyrenean mountains and larger settlements concentrated in the southern lowlands and along the main north–south transportation corridors. Together, these biophysical and settlement patterns strongly influence the occurrence and spread of predominantly human-caused wildfires across the region.

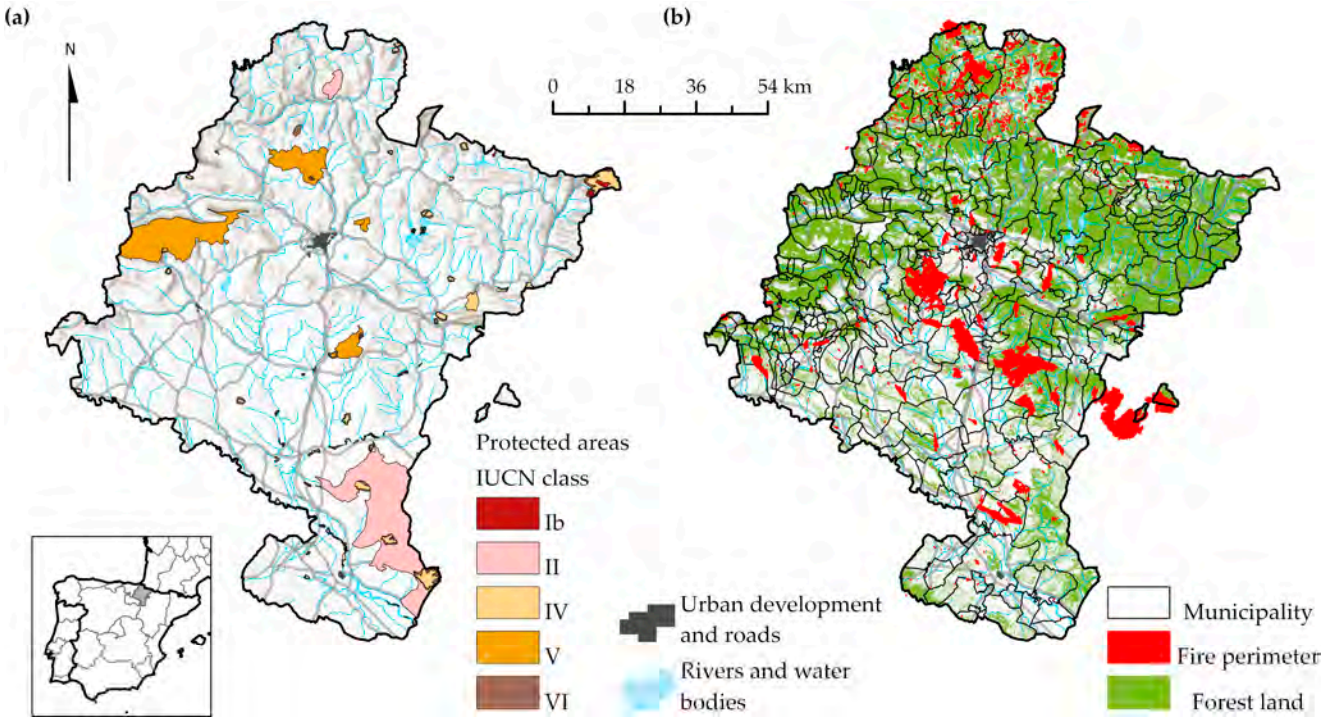

Figure 1. Protected areas classified by IUCN category (**a**) and municipal boundaries, forest land, and large fire perimeters (>100 ha) recorded during 1986–2024 in Navarra (10,391 km^2), northern Spain (**b**).

Wildfire ignitions in Navarra are predominantly human-caused, with lightning ignitions accounting for only 1.8% of total ignitions and 2.7% of total burned area in the 1984–2024 historical fire record. The largest burned areas are concentrated in the central mountainous sectors, whereas the northern part of the region is characterized by recurrent small pastoral fires [52]. The 2022 fire season was exceptional, with more than 17,000 ha burned and eight fires exceeding 250 ha. The largest events included the Arguedas fire on 19 June, which burned 2060 ha, the Legarda fire on 19 June, which burned 6248 ha, and the Gallipienzo fire on 20 June, which burned 6599 ha. These fires exhibited rapid growth, extreme behavior, and head-fire spread distances exceeding 10 km.

2.2. Fire Weather Conditions

To represent spatial variation in fire weather conditions across Navarra, the study area was divided into 20 pyromes (Appendix A). Pyrome delineation was based on physiographic, administrative, fire history, and landscape information, including watershed boundaries (n = 6313; mean area = 165 ha), the main river network, municipal and local administrative boundaries, climate, and historical large fire perimeters from 1986 to 2024. Pyromes were produced by progressively aggregating the watersheds into units of approximately 50,000 ha based on similarities across these variables and informed by expert knowledge from wildfire managers in the regional forest service. Outer boundaries were defined by major watershed divides or mountain ranges, large rivers, and administrative boundaries (Figure A1).

For each pyrome, the wildfire season was defined as the set of dates accounting for most of the burned area (>80% of the total burned area) based on 1986–2024 historical fire records (Table A1). The automatic weather station selected for each pyrome was the one with the longest record and valid hourly observations for at least 85% of the time series. When no station was available within the pyrome, stations located in neighboring regions with comparable physiographic and climatic conditions were used (Table A2). Hourly

records of wind direction, wind speed, temperature, solar radiation, precipitation, and fuel moisture variables were compiled from the selected stations.

Extreme fire weather scenarios used to model large fire spread were derived separately for each pyrome from the meteorological conditions observed during its wildfire season. Only records between 10:00 and 18:00 were used for wind characterization, as this interval represents the period of most active fire spread. Wind direction was summarized as the observed frequency of eight direction classes (45°, 90°, 135°, 180°, 225°, 270°, 315°, and 360°), and each direction class was assigned its corresponding 97th percentile wind speed (Table A3). Thus, wind direction was sampled according to observed wildfire season frequencies, whereas wind speed represented extreme active spread conditions within each direction class.

Fuel moisture scenarios were derived from the distribution of the Energy Release Component for fuel model G (ERC-G) for each pyrome. Fire Family Plus was used to estimate dead and live fuel moisture contents from the selected automatic weather station records [53,54]. Three ERC-G percentile scenarios were retained: the 70th, 85th, and 97th percentiles. Each scenario included separate fuel moisture values for 1 h, 10 h, and 100 h dead fuels and for live herbaceous and live woody fuels (Table A4). These scenarios were later sampled probabilistically during fire spread simulation, as described in Section 2.4 and Appendix D.

2.3. Landscape Fuels and Topography

The landscape file used for fire simulation was assembled at 50 m resolution from spatial fuel, canopy, and topographic layers. Surface fuels were first mapped by classifying vegetation according to shrub and forest height and composition, as described in Appendix B. Standard fuel models were then assigned to each vegetation type following Scott and Burgan [55], accounting for mean fuel height or depth, forest type (coniferous or broadleaved), climate zone (humid, Mediterranean, or semi-arid), and fire severity in areas affected by fires larger than 100 ha during the 2016–2024 period. Fire severity was classified into moderate- and high-severity classes to account for post-disturbance changes that occurred after the LiDAR acquisition used to characterize vegetation.

Canopy metrics were estimated at 50 m resolution by applying existing models based on 2016 LiDAR ALS data from the National Plan for Aerial Orography (PNOA) survey [56]. These models used LiDAR-derived metrics to estimate canopy cover (%), tree height (m), canopy base height (m), and canopy bulk density (kg m^{-3}) [57–59]. These metrics were subsequently adjusted in areas affected by moderate- and high-severity large fires. Topographic variables required for fire simulation, including slope, aspect, and elevation, were also derived. Finally, the fuel model, topographic, and canopy metric rasters were assembled into a multiband GeoTIFF landscape file at 50 m resolution within a 6 km buffer around the administrative boundary of Navarra. This extended domain improved model calibration and allowed the simulation of incoming fires originating beyond the study area limits.

2.4. Wildfire Modeling

Wildfire spread was simulated using the Minimum Travel Time (MTT) algorithm [60], implemented in the command-line version FConstMTT [61]. FConstMTT allows fire modeling conditions to be randomly sampled from observed probabilistic scenarios combining wind speed, wind direction, fuel moisture content, and fire duration, while ignition locations are distributed across the landscape using a spatially explicit ignition probability grid. The MTT algorithm models two-dimensional fire growth by identifying the set of pathways with minimum travel time from cell corners at a user-defined spatial resolution. Fire spread

is then calculated using Rothermel's surface fire spread model, and fireline intensity is converted to flame length using Byram's equation [62,63]. FConstMTT has been widely used in fire-prone regions to model wildfire spread and behavior across large landscapes and to assess wildfire exposure and risk to valued resources and assets [64,65].

The IP grid was generated at 50 m resolution using a logit occurrence model previously developed for central Navarra, with model performance of AUC = 0.772 and overall accuracy = 71% [51]. In this model, ignition probability is estimated as a function of distance to settlements, distance to power lines, population density, distance to railways, distance to roads, and land use. The resulting ignition probability surface showed the highest values near the road network and the most densely populated settlements, and it was used to distribute seed ignitions across the landscape. Because this ignition probability model was originally developed for central Navarra, we evaluated its regional transferability before applying it to the full simulation domain. The results of this external assessment, based on temporal and spatial holdout ignition datasets and random background points, are provided in Appendix C.

Simulations were performed at 50 m spatial resolution and organized by macroareas or pyroregions. Each macroarea was composed of one or several neighboring pyromes with similar fuels, topography, fire size distributions, and mean annual burned area. Fire-spread modeling was conducted independently for each macroarea, and the number of modeled years and simulated ignitions varied among macroareas to obtain spatially continuous and stable burn probability surfaces. Details on the macroarea structure, number of simulated ignitions, modeled years, historical annual burned area, and calibrated fire-spread durations are provided in Appendix D.

Ignitions were sampled from the ignition probability grid within each macroarea. For each simulated fire, fuel moisture conditions were randomly selected from the pyrome-specific ERC-G percentile scenarios, with 60% of fires assigned to the 97th percentile scenario, 30% to the 85th percentile scenario, and 10% to the 70th percentile scenario. Wind direction was sampled from the observed wildfire season frequency distribution for each pyrome, and wind speed was assigned as the 97th percentile value corresponding to the sampled wind direction. This configuration was designed to represent active fire spread conditions associated with large fire growth in Navarra rather than the full distribution of daily fire weather conditions.

Fire spread duration was calibrated independently for each macroarea to reproduce the historical fire size distribution and mean annual burned area derived from 38 years of fire records. Calibration was evaluated by comparing observed and modeled fire size distributions using fixed fire size classes, as reported in Appendix D. Annual burn probability layers were produced independently for each macroarea using macroarea-specific denominators and then assembled into the final regional mosaic.

Three burn probability metrics were derived from the simulations for each pixel i. Fireline intensity was first converted to flame length as

$$FL = 0.0775\ I^{0.46} \quad (1)$$

where FL is flame length (m) and I is fireline intensity (kW m^{-1}) [62]. Annual burn probability was then calculated as the proportion of modeled fire seasons in which pixel i burned under a given flame length threshold,

$$aBP_{i,\theta,m} = \frac{n_{i,\theta,m}}{N_m} \quad (2)$$

where $aBP_{i,\theta,m}$ is the annual burn probability for pixel i under flame length threshold θ in macroarea m, $n_{i,\theta,m}$ is the number of modeled years in which pixel i burned with

flame length greater than θ, and N_m is the macroarea-specific number of modeled years. The flame length thresholds were defined as $\theta = 0, 1.5,$ and 2.5 m. For $\theta = 0$, $aBP_{i,\theta,m}$ corresponds to annual burn probability. For $\theta = 1.5$ m, it corresponds to annual medium- and high-intensity burn probability. For $\theta = 2.5$ m, it corresponds to annual high-intensity burn probability. Thus, the three metrics quantify the expected annual likelihood of burning at increasing intensity levels, and, by definition,

$$aBP_{i,0,m} \geq aBP_{i,1.5,m} \geq aBP_{i,2.5,m} \quad (3)$$

2.5. Community Assets and Protected Areas

For the community-level analysis, spatial data included vector polygons representing the administrative boundaries of municipalities and other supramunicipal units without permanent settlements, including Bardenas Reales and Urbasa y Andía, across the entire territory of Navarra (10,391 km^2; n = 342; mean area about 3000 ha). Built assets were obtained from the Spanish National Topographic Database and included residential buildings (n = 228,005) and industrial structures (n = 21,987). The 2016 LiDAR data were used to build the fire simulation landscape file, whereas the 2024 LiDAR data were used to map current forest cover for exposure analysis. Forested areas within each administrative unit were delineated using a 25 m normalized digital surface model of vegetation height derived from the 2024 PNOA LiDAR dataset [66]. Areas with vegetation height greater than 3 m were classified as forested. These datasets were used to estimate exposure of built assets and forest land and to aggregate results at the municipal level.

For protected areas, spatial data consisted of vector polygons representing protected natural areas in Navarra (n = 172; mean area 540 ha). The dataset included Strict Nature Reserves, Natural Parks, Nature Reserves, Natural Enclaves, Protected Landscapes, Recreational Natural Areas, and their Peripheral Protection Zones and was compiled in accordance with the current regional legal framework governing protected areas in Navarra, including associated Natura 2000 sites. For each protected area, the analysis included the protected area code, name, type, and management category according to the IUCN classification system, with Peripheral Protection Zones assigned to Category VI. Forested areas within protected areas were delineated using the same 25 m normalized digital surface model of vegetation height, and areas with vegetation height greater than 3 m were classified as forested. These data were used to quantify wildfire exposure across the protected area network and its forested component.

2.6. Exposure Analysis

Wildfire exposure was assessed by intersecting simulated fire perimeters with community assets and protected areas across the study area. Exposure describes the spatial coincidence of values at risk with simulated fire footprints, but it does not quantify fire damage or loss [67]. All exposure metrics were calculated from the macroarea-specific annualized simulation outputs. Burned area, burned forest area, and estimated exposed structures were first averaged over the modeled years within each macroarea and then assembled or summed across macroareas to obtain regional and administrative unit summaries. This avoided pooling simulations under a single regional denominator and ensured that macroareas contributed according to their calibrated burned area regime rather than according to the raw number of simulated ignitions. Hereafter, all quantities expressed in year^{-1} refer to mean annual modeled values derived from the macroarea-specific annualized simulations.

For communities, exposure was quantified as the mean annual number of exposed residential buildings and industrial structures within each municipality using structure

centroids derived from the Spanish National Topographic Database [68]. For a given spatial unit m, annual exposure of structures was calculated as

$$aE_{u,c} = \sum_{m=1}^{M_u} \left(\frac{1}{N_m} \sum_{t=1}^{N_m} C_{u,c,m,t} \right) \quad (4)$$

where $aE_{u,c}$ is the mean annual number of exposed structures of class c in community u, M_u is the number of macroareas intersecting unit u, N_m is the macroarea-specific number of modeled years in macroarea m, and $C_{u,c,m,t}$ is the number of centroids of structure class c intersected by simulated fire perimeters in unit u, macroarea m, and modeled year t. Structure class c corresponds to residential buildings or industrial structures. Forest exposure within each community unit was quantified as mean annual burned forest area and calculated as

$$aBFA_u = \sum_{m=1}^{M_u} \left(\frac{1}{N_m} \sum_{t=1}^{N_m} FA_{u,m,t} \right) \quad (5)$$

where $aBFA_u$ is the mean annual burned forest area in community u, with M_u and N_m as defined above, and $FA_{u,m,t}$ is the forested area burned in unit u, macroarea m, and modeled year t. Forested area was defined as vegetation taller than 3 m and mapped at 25 m resolution using a 2024 LiDAR-derived digital surface model [66].

For protected areas, exposure was quantified as mean annual burned area for the total protected area and for its forested component. To account for fire intensity, burned area was also calculated for flame length thresholds of 1.5 m and 2.5 m. For a protected area p, annual burned area was calculated as

$$aBA_{p,\theta} = \sum_{m=1}^{M_p} \left(\frac{1}{N_m} \sum_{t=1}^{N_m} BA_{p,m,t,\theta} \right) \quad (6)$$

where $aBA_{p,\theta}$ is the mean annual burned area in protected area p under flame length threshold θ, M_p is the number of macroareas intersecting protected area p, N_m is the macroarea-specific number of modeled years, and $BA_{p,m,t,\theta}$ is the area burned in protected area p, macroarea m, and modeled year t with flame length exceeding threshold θ, using the same flame length thresholds defined above. The term $aBA_{p,m,t,\theta}$ refers to a burned area where simulated flame length was greater than θ; therefore, the condition $FL > \theta$ is included in the threshold-specific burned area variables. Burned forested area within protected areas was calculated analogously as

$$aBFA_{p,\theta} = \sum_{m=1}^{M_p} \left(\frac{1}{N_m} \sum_{t=1}^{N_m} FA_{p,m,t,\theta} \right) \quad (7)$$

where $aBFA_{p,\theta}$ is the mean annual burned forest area in protected area p under flame length threshold θ, with M_p and N_m as defined above, and $FA_{p,m,t,\theta}$ is the forested area burned in protected area p, macroarea m, and modeled year t with flame length exceeding threshold θ. The term $FA_{p,m,t,\theta}$ refers to burned forest area where simulated flame length was greater than θ; therefore, the condition $FL > \theta$ is included in the threshold-specific burned forest area variables. Exposure metrics were annualized within each macroarea using macroarea-specific denominators and then summarized separately for communities and protected areas.

3. Results

3.1. Burn Probabilities and High-Intensity Fire Potential

Burn probability exhibited complex spatial patterns across Navarra as a result of the interaction among ignition source areas, fire weather conditions, and the simulated distributions of fire size and frequency (Figure 2a). The highest values were concentrated in

central–eastern Navarra, where complex terrain, fuel accumulation, and severe fire weather conditions favored the occurrence and spread of large fires, consistent with the distribution of observed large fire perimeters (Figure 1). Within this area, some recently burned zones showed lower burn probability because reduced fuel loads limited subsequent fire spread, particularly in the core of the central burned areas where modeled fires showed limited penetration. In southern Navarra, extensive irrigated agricultural lands substantially constrained fire spread, whereas higher burn probability values were concentrated in adjacent rainfed agricultural areas. Additional high-probability patches occurred in northern sectors, particularly on slopes and higher-elevation pastoral areas, where shrub-dominated fuels and high ignition frequency along mountain ridges produced locally elevated burn probability. The lowest burn probability values were found in the northeastern Pyrenees, where fire frequency is low and large fires are rare.

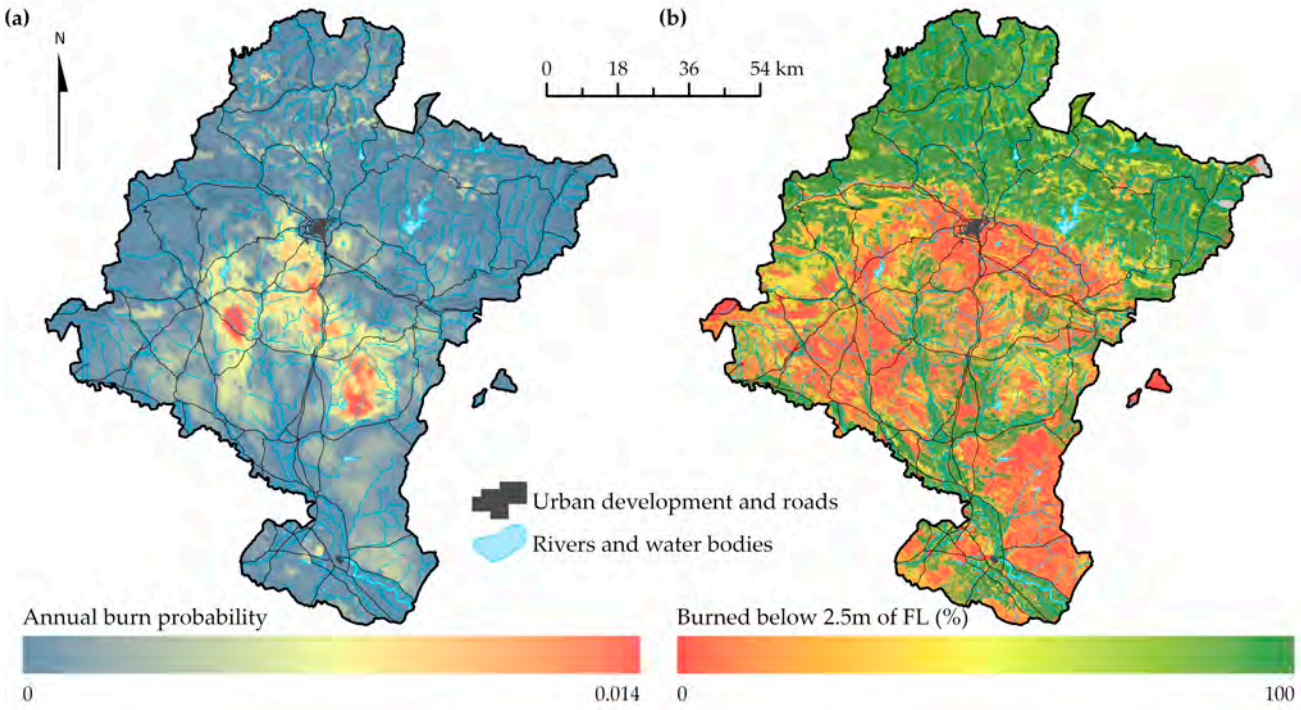

Figure 2. Modeled maps of annual burn probability (**a**) and the percentage of burn occurrences with flame length below 2.5 m (**b**) across Navarra. Annual burn probability showed clear hotspots in central Navarra, whereas the highest proportions of lower-intensity burning occurred in the northern and Pyrenean sectors.

The conditional fire intensity metric identifies where, given that a pixel burned, simulated fire more often remained below the 2.5 m flame length threshold; higher values indicate a greater proportion of lower-intensity burning, whereas lower values indicate a greater tendency toward high-intensity fire (Figure 2b). This pattern was especially evident in timber litter fuels and grasslands of the northern sectors, where comparable burn probability levels were associated with lower modeled fire intensity. In contrast, complex terrain produced sharp local transitions in high-intensity burn probability, reflecting the interactions among slope, aspect, and fire spread direction. These contrasts were most evident between areas burned under head fire conditions and adjacent locations where flanking and backing fire produced substantially lower intensity. Similar sharp transitions were also associated with abrupt changes in fuel conditions, particularly along boundaries between grasslands and highly hazardous shrublands, where high-intensity burn probability increased markedly.

3.2. Community Exposure to Wildfire

Exposure of residential structures to simulated wildfire was highly uneven across Navarra (Appendix E; Figure 3a). The mean annual number of exposed residential buildings summed to 120 structures yr^{-1}, with values ranging from 0 to 4.7 structures yr^{-1} among administrative units. The highest residential exposure occurred in municipalities located in fire-prone sectors of central, central–eastern, and northwestern Navarra, including Valle de Yerri in the west–central region, Baztan in the northwest, Cizur in the central Pamplona corridor, Ultzama in the north–central sector, and Ujué and Tafalla in the central–eastern and south–central sectors, respectively. Additional high values were observed in San Martín de Unx and Galar. In contrast, the lowest residential exposure values were concentrated in the northeastern Pyrenees and other low-fire-activity sectors, including municipalities such as Garde and Urzainqui. High residential exposure did not necessarily occur in the municipalities with the largest building inventories. For example, major urban municipalities such as Pamplona and Tudela contained much larger numbers of residential structures than many of the most exposed municipalities, yet their modeled annual exposure was lower. This pattern indicates that residential exposure was driven more strongly by the spatial interaction between settlement location and modeled fire transmission than by structure abundance alone. Residential exposure was strongly concentrated across administrative units: 68 municipalities accounted for 75% of the modeled annualized exposure of residential buildings while covering 37% of the total municipal area and containing 37% of the regional residential building stock. This indicates that modeled residential exposure was not simply proportional to either municipal area or the number of residential buildings (Figure 4a).

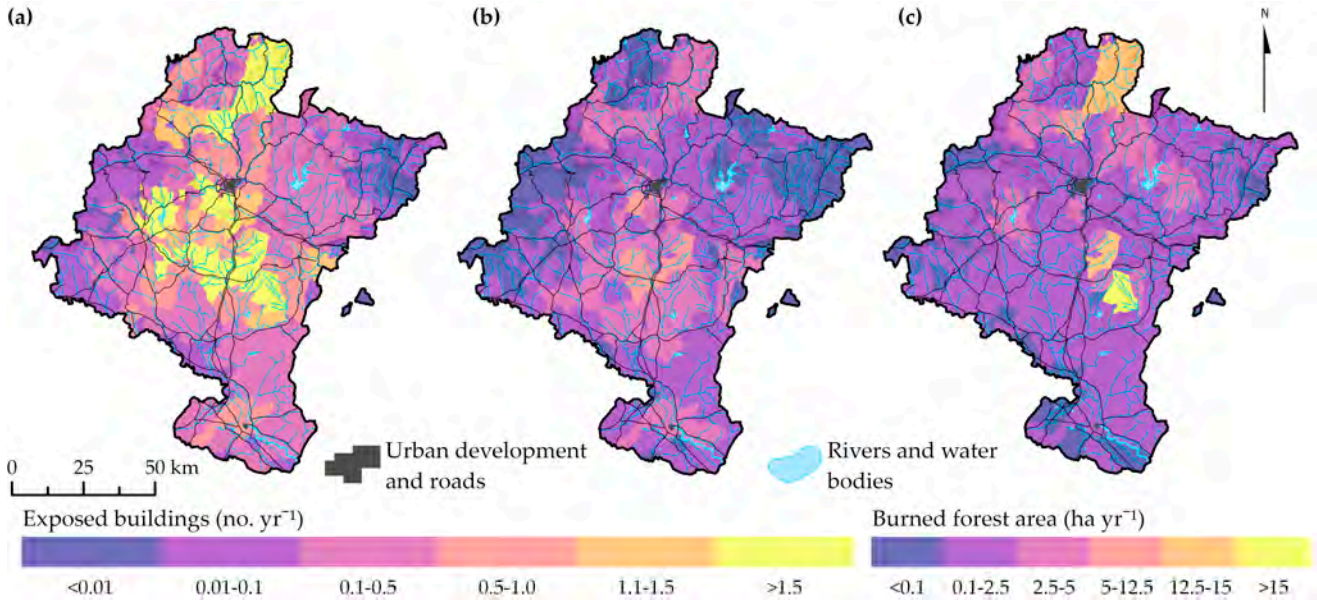

Figure 3. Wildfire exposure of (**a**) residential structures, (**b**) industrial structures, and (**c**) forest land across Navarra. See Table A8 for community-level exposure data for structures and forest land.

A similar pattern was observed for industrial structures, although overall values were lower (Appendix E; Figure 3b). The mean annual number of exposed industrial structures summed to 15.74 structures yr^{-1}, with values ranging from 0 to 0.63 structures yr^{-1}. The highest industrial exposure occurred in municipalities distributed across central and south–central Navarra, including Tafalla, Artajona, Leoz, Cizur, and Ujué, together with north–central municipalities such as Ultzama and west–central units such as Valle de Yerri. Elevated values were also observed in Barásoain and Caparroso. The lowest industrial

exposure values were concentrated in the northeastern Pyrenees and other low-fire-activity sectors, including Urzainqui, Uztárroz, Esparza de Salazar, and Garde. As with residential exposure, municipalities with the largest industrial building inventories did not necessarily show the highest modeled exposure. For example, Tudela and other municipalities with large industrial inventories ranked below several smaller municipalities embedded within landscapes characterized by higher burn probability and stronger simulated fire transmission. Industrial exposure showed a similar administrative concentration: 56 municipalities accounted for 75% of the modeled annualized exposure of industrial structures while covering 35.8% of the total municipal area and containing 50.6% of the industrial structure stock. As with residential exposure, municipalities with the largest industrial inventories were not necessarily those with the highest modeled wildfire exposure (Figure 4b).

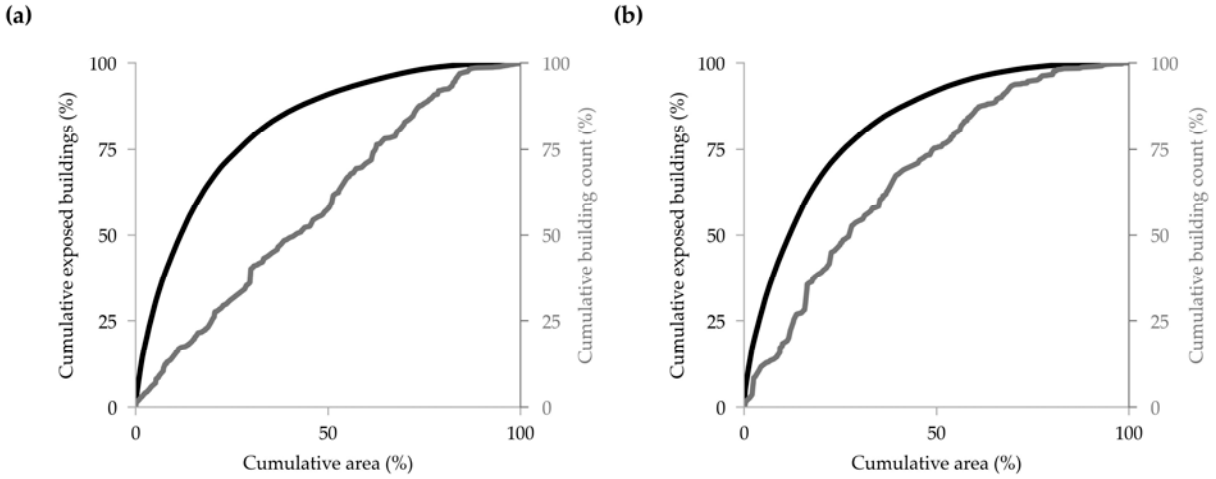

Figure 4. Cumulative modeled annualized wildfire exposure and structure counts for (**a**) residential buildings and (**b**) industrial structures across municipalities in Navarra. Municipalities are ranked by decreasing wildfire exposure per unit area. The black line represents cumulative exposure, and the gray line represents cumulative structure counts. The curves distinguish concentration of exposure, municipal area, and structure inventory, showing that exposure is more spatially concentrated than either area or asset abundance alone.

Exposure of forest land, expressed as mean annual burned forest area, also showed strong spatial concentration (Appendix E; Figure 3c). Across Navarra, mean annual burned forest area summed to 235 ha yr^{-1}. The highest values were found in municipalities of the central–eastern and northwestern mountain landscapes, including Ujué, Leoz, and Olóriz in the central-eastern sector and Baztan, Ultzama, Basaburua, Goizueta, and Esteribar in the northern and northwestern sectors. Additional high values occurred in west–central municipalities such as Valle de Yerri and Cirauqui. In contrast, the lowest forest exposure values were generally associated with densely urbanized municipalities and southern agricultural landscapes, where limited forest cover and strong landscape discontinuities constrained modeled fire spread. Overall, the municipal pattern of forest exposure was consistent with the regional burn probability patterns, with the highest values concentrated in mountainous areas with greater fuel continuity and recurrent large fire transmission (Figure 3c).

3.3. Protected Area Exposure to Wildfire

Wildfire exposure across the protected area network was highly uneven and concentrated in a limited number of large units and protected area types (Appendix F; Table 1). Across all protected areas, mean annual burned area summed to 90 ha yr^{-1} after counting overlapping protected area polygons only once. Of this total, 81 ha yr^{-1} occurred at flame

lengths greater than 1.5 m and 68 ha yr^{-1} at flame lengths greater than 2.5 m. At the type level, Natural Parks accounted for the largest share of total exposure, with 56 ha yr^{-1}, followed by Protected Landscapes, with 29 ha yr^{-1}. Peripheral Protection Zones and Nature Reserves contributed substantially lower totals, whereas Natural Enclaves, Recreational Natural Areas, and Strict Nature Reserves showed very limited annual burned area. This pattern indicates that total protected area exposure was dominated by a small number of extensive units embedded within landscapes of high burn probability and recurrent large fire transmission.

Table 1. Summary of modeled wildfire exposure by protected area type in Navarra. Values are summed across all units within each protected area type and include total mean annual burned area, burned area at flame lengths greater than 1.5 m and 2.5 m, and the corresponding burned forest area metrics. Abbreviations: aBA = mean annual burned area; aBFA = mean annual burned forest area. In the Total row, overlapping areas among protected area types were counted only once to avoid double-counting exposure across the regional protected area network.

Protected Area Type	No. of Units	Total Area (ha)	aBA (ha yr^{-1})	$aBA_{1.5}$ (ha yr^{-1})	$aBA_{2.5}$ (ha yr^{-1})	aBFA (ha yr^{-1})	$aBFA_{1.5}$ (ha yr^{-1})	$aBFA_{2.5}$ (ha yr^{-1})
Natural Parks	3	64,511.6	55.50	53.37	48.71	2.18	1.48	1.14
Protected Landscapes	4	12,415.9	28.86	22.94	15.75	12.61	8.79	6.19
Peripheral Protection Zones	94	5239.8	5.65	4.90	3.77	1.21	0.99	0.72
Nature Reserves	38	9045.6	3.85	3.42	2.65	1.67	1.44	1.15
Natural Enclaves	28	1050.9	0.66	0.49	0.34	0.47	0.35	0.24
Recreational Natural Areas	2	446.9	0.18	0.07	0.02	0.13	0.03	0.00
Strict Nature Reserves	3	553.0	0.02	0.00	0.00	0.01	0.00	0.00
Total	172	93,263.7	89.90	81.06	67.86	15.63	10.75	7.43

At the unit level, the highest total exposure occurred in Bardenas Reales, located in southern Navarra, with 50 ha yr^{-1} burned on average (Figure 5). This value was markedly higher than for any other protected area and was also associated with very high modeled fire intensity, with 49 ha yr^{-1} burned at flame lengths greater than 1.5 m and 45 ha yr^{-1} at flame lengths greater than 2.5 m. The second highest total exposure was observed in Montes de Valdorba, a Protected Landscape in central–eastern Navarra, with 16.23 ha yr^{-1}, followed by Robledales de Ultzama y Basaburua in north–central Navarra, with 12.26 ha yr^{-1}, and Sierras de Urbasa y Andía in west–central Navarra, with 5 ha yr^{-1}. Additional units with comparatively elevated exposure included surroundings of Laguna de Pitillas, Monte del Conde, and Vedado de Eguaras, although values dropped sharply below those of the four most exposed areas. In contrast, the lowest exposure values were found in small reserves, recreational natural areas, and peripheral units located in the northeastern Pyrenees and in low-fire-activity riparian or wetland environments.

Exposure of forested land within protected areas followed a different pattern from that observed for total burned area (Figure 5). Across the protected area network, mean annual burned forest area summed to 16 ha yr^{-1} after counting overlapping protected area polygons only once, including 11 ha yr^{-1} at flame lengths greater than 1.5 m and 7 ha yr^{-1} at flame lengths greater than 2.5 m. In this case, Protected Landscapes accounted for the largest share of forest exposure, with 13 ha yr^{-1}, clearly exceeding Natural Parks (2.1 ha yr^{-1}) and Nature Reserves (1.7 ha yr^{-1}). The highest burned forest area occurred in Montes de Valdorba, with 7 ha yr^{-1}, followed by Robledales de Ultzama y Basaburua, with 4.92 ha yr^{-1}, and Sierras de Urbasa y Andía, with 0.96 ha $year^{-1}$. Although Bardenas Reales dominated total protected area exposure, its burned forest area was comparatively low (0.8 ha yr^{-1}), reflecting the predominance of open dryland vegetation rather than extensive tree cover. High-intensity burned forest area was concentrated in the same

wooded units, particularly Montes de Valdorba, which also showed the highest values for forest area burned at flame lengths greater than 1.5 m and 2.5 m. Overall, the protected areas with the highest total burned area were not necessarily those with the highest burned forest area. This contrast was especially evident between Bardenas Reales, which dominated total exposure, and Montes de Valdorba and Robledales de Ultzama y Basaburua, which dominated exposure of forested land. The results therefore show that total protected area exposure and forest exposure were only partially coincident across the network and that fire intensity adds an important dimension for distinguishing protected areas exposed primarily to extensive burning from those exposed to higher-severity impacts on forest ecosystems.

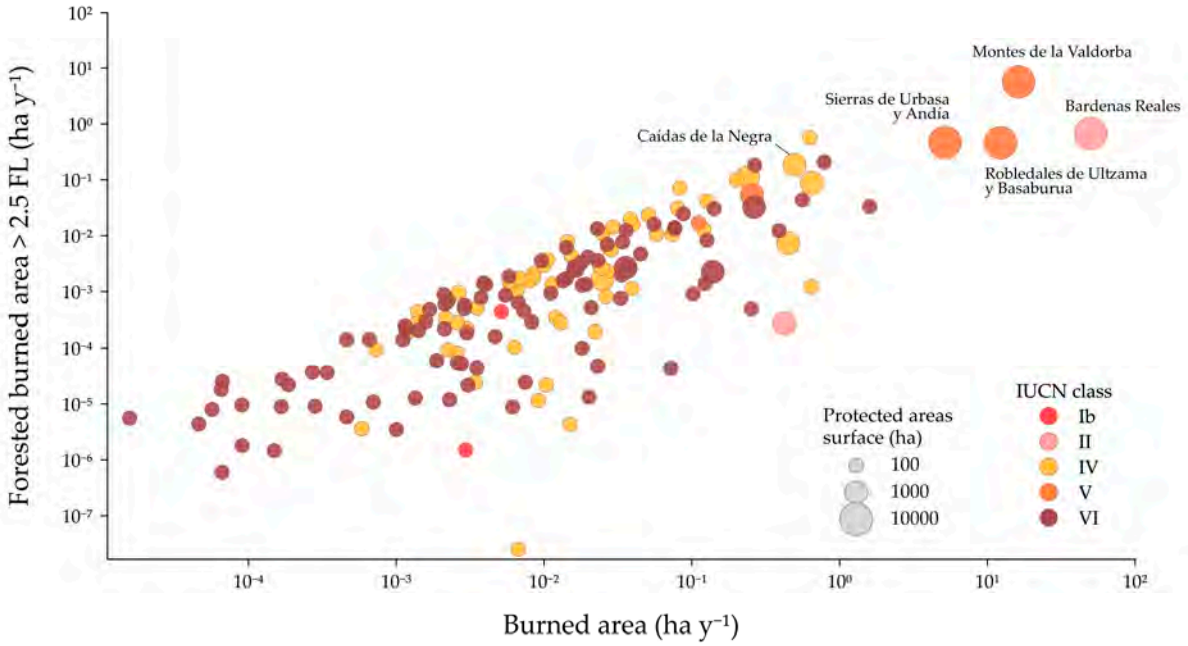

Figure 5. Scatterplot of mean annual burned area versus mean annual burned forest area at flame lengths greater than 2.5 m for protected areas in Navarra. Bubble color indicates IUCN category, and bubble size represents the area of protected areas. See Table A9 for protected area exposure data for total and forested area across different fire intensity classes.

4. Discussion

This study provides the first regional-scale assessment of wildfire exposure to communities and protected areas throughout Navarra, Spain. By integrating pyrome-specific fire weather conditions, historical ignition patterns, spatial fuels, and topography within a fire modeling framework, the analysis captured strong spatial variability in wildfire likelihood, expected fire intensity, and structure exposure across the region. This represents an important advance over historical event-based assessments, as simulations can predict potential burn patterns, fire intensity, and exposure in areas where future fires may differ from the limited historical record [39,45,46]. While empirical assessments of wildfire activity rely on smoothed maps of spatial patterns of historical ignitions, simulations provide fine-scale burn probability and intensity maps that can be used to identify where communities, forest land, and protected areas are more likely to be affected by large fire events, thereby accounting for transmission pathways that are not captured by ignition location alone [36,50,69]. The Navarra case study demonstrates the integration of regional fire history data, spatial fuels, weather scenarios, and asset layers to support risk-based prioritization of community protection, protected area management, and landscape-scale fuel treatments.

Although this study focused on the province of Navarra, the modeling framework is relevant to other fire-prone regions globally where extreme fire weather, fuel accumulation, land use change, and expanding wildland–urban interfaces are all contributing to a rapid increase in wildfire impacts to a wide range of human and ecological values [70]. We used a pyrome framework to stratify Navarra into homogeneous zones with respect to fire regime across a highly heterogeneous region. Pyromes with the highest burned area and strongest concentration of large fire activity are the locations where simulation outputs are likely to be most useful for treatment design, contingency planning, and evaluation of landscape interventions. In this sense, the study provides not only exposure estimates but also a spatial framework for future scenario analysis and management testing.

We found that the highest wildfire exposure in Navarra is strongly concentrated in central–eastern sectors where complex terrain, fuel accumulation, and severe fire weather conditions contribute to higher burn probability. In contrast, simulation outputs predicted relatively low burn probability in the northeastern Pyrenees and in the extensive irrigated agricultural areas to the south. These spatial patterns were consistent with the historical distribution of large fire perimeters and highlight the combined influence of ignition sources, fire weather, landscape configuration, and post-fire fuel conditions on modeled fire transmission. The concentration of burn probability and high-intensity burn probability in a limited fraction of the territory suggests that regional prevention efforts are likely to be most effective when directed to specific zones rather than distributed evenly across the landscape [71]. As suggested in several other studies, burn probability hotspots can identify priorities where strategic fuel treatments and other mitigation actions are most likely to reduce wildfire exposure and transmission [43,44,71–73].

For residential and industrial structures, the results indicate that wildfire exposure is concentrated in a relatively small portion of Navarra. Three fourths of modeled residential and industrial exposure was concentrated in 68 and 56 municipalities, respectively, covering about 37% and 36% of the total municipal area. Both residential and industrial exposure were higher in municipalities located in central, central–eastern, north–central, and northwestern Navarra and lower in the northeastern Pyrenees. Predicted exposure did not always coincide with municipalities with the largest numbers of structures (Table A8). Large urban centers such as Pamplona and Tudela have a higher number of buildings than other municipalities with higher overall exposure, a finding that underscores the importance of building arrangement and density in relation to wildland fuels [74,75]. Prior work to understand and classify WUIs based on their permeability to fire has led to WUI archetypes and the finding of particular densities that optimize wildfire exposure to buildings [76].

Our results are broadly consistent with the planning logic of INFONA 2022, Navarra's civil protection emergency plan for forest fires, which uses relatively coarse municipal-scale risk and vulnerability zoning to determine where municipal wildfire action plans are mandatory or recommended [77]. These plans define local preparedness, emergency organization, evacuation procedures, interface area identification, and available suppression resources. Agreement between the two approaches is strongest in municipalities where buildings are intermixed with fuels in higher burn probability areas, whereas discrepancies were most apparent in higher-density, larger municipalities with lower predicted exposure. Wildfire protection planning in Navarra can benefit from future work to integrate information from wildfire simulation into INFONA and thus potentially refine territorial civil protection zoning and local planning using predicted fire events to prioritize fuel treatments and other protection investments.

Our results can also inform the Government of Navarra's Subregional Forest Plans (PFCs), which define forest management guidelines and planning priorities across broader

forest-management regions. The PFCs are organized into separate reference documents for the Cantabrian, Pyrenean, and Middle Zone–Ribera subregions. In this context, our fine-scale maps of burn probability and fire intensity exposure can help identify where forest management could be prioritized within each planning region to reduce impacts to forest resources. For instance, simulation outputs predicted higher burn probability and intensity in central–eastern and northwestern mountain landscapes corresponding to the Middle Zone subregion. Similarly, the results can also inform fire management to conserve protected areas where we observed substantial variability among the different parcels and protected-area types. Total exposure was dominated by Natural Parks and, at the unit level, by Bardenas Reales, which substantially exceeded all other protected areas in mean annual burned area, and in burned area at moderate and high intensity. However, the pattern changed when only forested land was considered, with burned forest area concentrated mainly in protected landscapes, such as Montes de Valdorba. This contrast shows that total protected area exposure and forest exposure were only partially coincident, highlighting the need to separate total burned area from burned forest area, especially in dryland protected areas with limited tree cover. Fire intensity adds an important dimension because high-intensity burned forest area identifies wooded protected areas where fire may produce substantial structural effects, while lower-intensity burning may contribute to vegetation renewal and fuel regulation in Mediterranean fire-adapted systems [78]. Thus, burn probability and fire intensity outputs can identify candidate areas for restoration-oriented fuel management or managed fire evaluation, but any fire reintroduction would require local assessment of conservation status, ecosystem-specific effects, and appropriate burn magnitude, seasonality, and recurrence [79–81].

We recognize several limitations in the application of wildfire simulation models and the underlying uncertainty in the outputs [82–84]. Although simulated fire events were calibrated to reproduce observed fire size distributions and mean annual burned area by macroarea, the resulting annual burn probabilities and exposure estimates should be interpreted as model-based decision support estimates rather than independently validated predictions. The outputs are conditioned on the historical fire occurrence record, the transferred ignition probability surface, the fuel and canopy layers, the pyrome-specific fire weather and fuel moisture scenarios, and the calibration assumptions used for each macroarea. In addition, fuels and canopy attributes were derived from LiDAR and subsequently adjusted for recent disturbances, which means that exposure estimates remain dependent on the quality and temporal accuracy of those inputs [85]. Fuel conditions and canopy structure will continue to change in the region in response to wildfires, land use change, vegetation growth, and forest management [86]. Therefore, continued application of the modeling framework will require periodic updates, preferably at intervals shorter than 10 years or after major disturbance events. Despite these limitations, the outputs provide useful spatially explicit information to support wildfire management decisions at multiple scales within Navarra.

5. Conclusions

This study contributes to improving wildfire management in Navarra by using wildfire simulation modeling to map potential wildfire exposure, thereby providing a basis for transitioning from a reactive response to risk-informed prevention. Overall, the approach provides a scalable decision support framework for prioritizing mitigation, preparedness, and landscape planning under increasing wildfire pressure in Navarra. Future work can use these simulation outputs for strategic fuel treatment design and project prioritization in Navarra [87]. Fire simulations can be refined for local areas and used to test alternative landscape treatment configurations by simulating fuel management on the ground and

re-simulating large numbers of wildfire scenarios. Likewise, ongoing fuel management activities in Navarra can use the existing simulation outputs to examine the extent to which predicted fire events will intersect with treated areas, thereby potentially improving the scheduling and prioritization of strategic management areas and fuel breaks across the region [88].

Author Contributions: Conceptualization, F.A., A.A., C.M., and M.R.; methodology, F.A. and A.A.; software, A.A.; model calibration and evaluation, F.A.; formal analysis, F.A., J.L., and I.P.; resources, P.G. and I.G.; data curation, P.G., I.G., J.L., and I.P.; writing—original draft preparation, F.A.; writing—review and editing, A.A. and P.G.; visualization, J.L. and I.P.; project administration, F.A.; funding acquisition, F.A., C.M., and M.R. All authors have read and agreed to the published version of the manuscript.

Funding: This research was funded by the ANDIA 2023 Senior Talent Attraction call, Grant No. 0011-3947-2022-000001, funded by the Government of Navarra, and by LIFE-IP NAdapta-CC, Grant No. LIFE16 IPC/ES/000001, funded by the European Commission.

Data Availability Statement: Stochastic wildfire modeling probabilistic risk estimates can be downloaded at https://zenodo.org/records/14615748 (Accessed on 11 November 2025.). Exposure to communities can be downloaded at https://zenodo.org/records/17495885 (Accessed on 11 November 2025). Exposure to protected areas can be downloaded at https://zenodo.org/records/17583829 (Accessed on 11 November 2025.).

Acknowledgments: The authors thank Stuart Brittain, of Alturas Solutions, for adapting the FConstMTT wildfire simulator, developed by the Missoula Fire Sciences Laboratory of the USDA Forest Service, for use in this study. The simulator is available at Missoula Fire Lab Command Line Applications: https://www.alturassolutions.com/FB/FB_API.htm. The authors also thank MeteoNavarra for providing complete hourly records from the automatic weather station network in Navarra and the Department of Rural Development and Environment of the Government of Navarra for providing the regional fire reports and ignition records used in this study.

Conflicts of Interest: The authors declare no conflicts of interest.

Abbreviations

The following abbreviations are used in this manuscript:

IUCN	International Union for Conservation of Nature
MTT	Minimum Travel Time
LiDAR	Light Detection and Ranging
ERC	Energy Release Component
I	Fireline intensity
FL	Flame length
E	Exposed structures
aBP	Annual burn probability
aBA	Annual burned area
aBFA	Annual burned forest area
PAMIF	Planes de Actuación Municipales por Incendios Forestales
PFC	Planes Forestales Comarcales

Appendix A. Fire Regime Description and Weather Conditions in the Pyromes

The study area was divided into pyromes with homogeneous fire regime conditions to characterize fire weather conditions and support wildfire modeling (Figure A1). Most of the observed burned area was concentrated in central and northern Navarra, particularly in pyromes 1, 14, and 15, where the mean annual burned area exceeded 0.4% of the pyrome

area (Table A1). In pyromes 16 and 11, lightning-caused fires accounted for more than 10% of the total burned area. Pyromes 1 and 20 had the highest ignition densities. The recurrence of fires larger than 100 ha varied among pyromes, while fires larger than 1000 ha were infrequent. Seasonal patterns of fire occurrence also differed across the study area. In northern Navarra, fires occurred mainly in autumn and winter, whereas in central Navarra fire activity was concentrated in the summer months. In southern Navarra, fire occurrence was distributed across most of the year.

The automatic weather stations used in the analysis are listed in Table A2. Stations located on ridges, summits, or ravine bottoms were excluded, and preference was given to stations in open valleys outside of urban areas. The data series were reviewed and converted to the text format (*.fw9) required for processing in Fire Family Plus [53]. For some pyromes, no suitable internal weather station was available within the pyrome. In these cases, the nearest station with comparable physiographic and climatic conditions was used; pyromes 4 and 8 inherited the weather scenarios from pyrome 7.

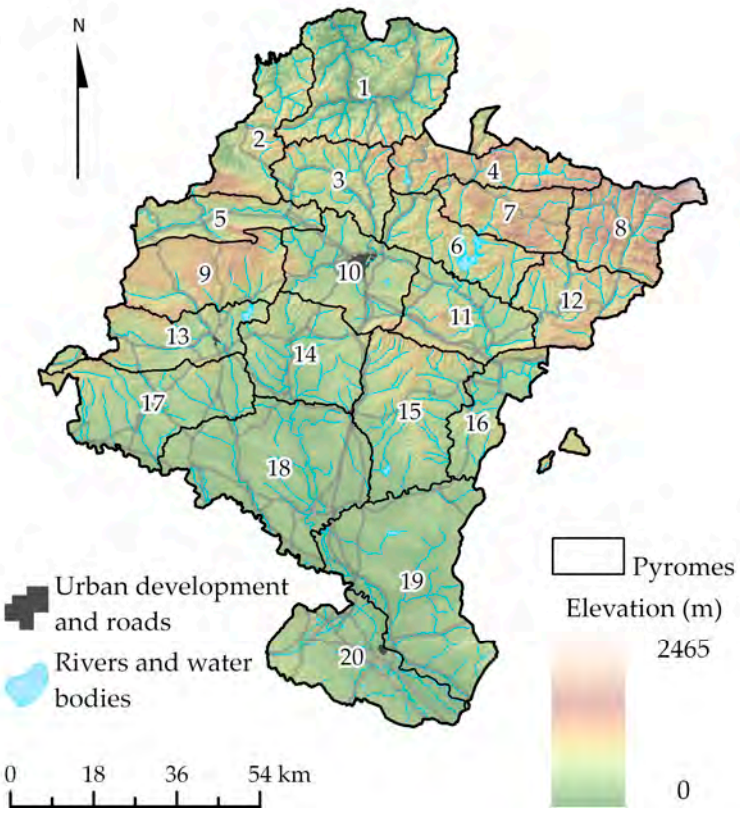

Figure A1. Delineation of 20 pyromes with homogeneous fire regime conditions in Navarra (mean area = 52,000 ha). This segmentation was used to characterize historical fire size distributions and associated fire weather scenarios for wildfire simulation with FConstMTT.

For pyromes without a suitable internal automatic weather station, weather and fuel moisture scenarios were assigned from the nearest neighboring pyrome with comparable elevation, vegetation, and fire weather conditions. This applied to pyromes 4 and 8, which inherited the wind and fuel moisture scenarios used for their corresponding neighboring pyrome, rather than being treated as independent weather station records.

Table A1. Fire regime characteristics of the 20 pyromes defined in Navarra. Burned area is expressed as the mean annual percentage of pyrome area burned; values in parentheses indicate the percentage of total burned area attributed to lightning-caused fires. Ignition density is expressed as the annual number of ignitions per km^2, and large wildfires are defined as fires larger than 100 ha. The wildfire season corresponds to the dates accounting for more than 80% of the total burned area.

Pyrome (Code)	Area (ha)	Burned Area (% $year^{-1}$)	Ignitions (no. km^{-2} $year^{-1}$)	Large Fires (no. $year^{-1}$)	Wildfire Season (Dates)
Bidasoa (1)	82,750	0.41 (0.01)	0.059	0.58	15 December to 20 April
Urumea (2)	40,625	0.05 (<0.01)	0.015	0.03	5 September to 30 April
Ulzama (3)	38,367	0.03 (0.42)	0.016	0.00	1 February to 15 April
Irati-Alduides (4)	36,840	0.02 (<0.01)	0.007	0.03	15 October to 25 April
Barranca (5)	31,927	0.03 (<0.01)	0.030	0.00	20 July to 25 March
Itoiz y Valle Erro medio (6)	38,065	0.01 (0.31)	0.008	0.00	1 September to 20 February
Alto Valle Salazar y Lintzoain (7)	32,460	0.03 (0.96)	0.018	0.00	1 January to 25 April
Norte Valle del Roncal (8)	43,350	0.01 (6.28)	0.003	0.00	1 January to 20 February
Sierra de Urbasa (9)	50,600	0.01 (0.99)	0.005	0.00	25 June to 25 September
Cuenca de Pamplona (10)	50,430	0.21 (2.16)	0.031	0.21	20 June to 30 September
Peña Izaga y Lumbier (11)	41,034	0.09 (12.71)	0.010	0.05	20 July to 20 August
Valles bajos Roncal y Salazar (12)	35,901	0.01 (0.91)	0.004	0.00	1 March to 10 April
Tierra Estella norte (13)	39,900	0.04 (0.01)	0.021	0.08	25 June to 20 September
Entorno Puente la Reina (14)	51,515	0.60 (1.44)	0.024	0.24	15 June to 25 June
Macizo zona media (15)	66,951	0.40 (1.55)	0.018	0.21	20 June to 25 August
Sierra Peña de Leire (16)	32,001	0.25 (53.92)	0.015	0.13	15 June to 15 August
Tierra Estella sur (17)	64,057	0.10 (0.67)	0.023	0.11	20 June to 20 August
Ribera alta (18)	98,518	0.08 (0.50)	0.035	0.16	15 June to 10 September
Bardenas Reales (19)	101,300	0.11 (1.72)	0.018	0.08	20 June to 25 July
Ribera baja (20)	62,191	0.08 (0.19)	0.070	0.00	15 January to 10 November

Table A2. Automatic weather stations used to characterize meteorological conditions for each pyrome. The number of years with at least 90% of hourly records is indicated. Pyromes 4 and 8 did not have suitable internal station records and were assigned weather scenarios from pyrome 7 due to comparable physiographic and fire weather conditions.

Pyrome Code	Station Name (Code)	Latitude (°)	Longitude (°)	Elevation (m)	Years
1	Doneztebe (42)	43.12959	−1.66495	128	21
2	Aralar (22)	42.95253	−1.96435	1344	19
3	Oskotz (37)	42.95498	−1.75740	562	21
4	Erremendia (249), inherited from pyrome 7	42.87778	−1.18510	1050	inherited
5	Etxarri-Aranatz (8)	42.90844	−2.05966	505	27
6	Aoiz (34)	42.7904	−1.37018	534	26
7	Erremendia (249)	42.87778	−1.18510	1050	18
8	Erremendia (249), inherited from pyrome 7	42.87778	−1.18510	1050	inherited
9	Trinidad de Iturgoien (29)	42.81215	−1.98259	1224	18
10	Arazuri (243)	42.80976	−1.72318	396	16
11	Lumbier (247)	42.66532	−1.27572	484	18
12	Arangoiti (23)	42.6447	−1.1956	1352	15
13	Estella (7)	42.67458	−2.02751	485	24
14	Artajona (264)	42.58354	−1.79083	359	17
15	Ujué (30)	42.51163	−1.51100	829	19
16	Yesa (10)	42.61738	−1.19155	487	27
17	Bargota (268)	42.47948	−2.29795	385	25
18	Falces (269)	42.42280	−1.79244	297	16
19	Bardenas (El Yugo) (31)	42.20460	−1.58321	486	16
20	Cascante (276)	42.03621	−1.72270	337	16

Wind frequency during the fire period was calculated for eight wind directions (45°, 90°, 135°, 180°, 225°, 270°, 315°, and 360°) within the 10:00–18:00 time window, along with the corresponding 97th percentile wind speeds (Table A3).

Table A3. Wind frequency (%), with 97th percentile wind speed (km h^{-1}, in parentheses), for each wind direction in each pyrome. Pyromes without suitable internal weather station records are shown explicitly and report the wind scenarios inherited from their assigned neighboring pyrome, as indicated in Table A2.

Pyrome (Code)	45°	90°	135°	180°	225°	270°	315°	360°
Bidasoa (1)	4 (18)	5 (14)	16 (16)	16 (16)	17 (14)	22 (14)	12 (19)	8 (19)
Urumea (2)	3 (35)	2 (34)	8 (35)	20 (35)	16 (35)	10 (35)	24 (35)	18 (35)
Ultzama (3)	7 (14)	10 (14)	7 (11)	10 (13)	20 (18)	27 (19)	14 (16)	3 (14)
Irati-Alduides (4), inherited from 7	2 (23)	8 (23)	16 (26)	14 (19)	15 (19)	17 (14)	20 (18)	7 (23)
Barranca (5)	6 (19)	7 (31)	12 (35)	15 (34)	10 (19)	27 (19)	21 (19)	3 (19)
Itoiz y Valle Erro Medio (6)	4 (23)	6 (19)	20 (26)	16 (19)	19 (19)	16 (23)	14 (19)	4 (26)
Alto Valle Salazar y Lintzoain (7)	2 (23)	8 (23)	16 (26)	14 (19)	15 (19)	17 (14)	20 (18)	7 (23)
Norte Valle del Roncal (8), inherited from 7	2 (23)	8 (23)	16 (26)	14 (19)	15 (19)	17 (14)	20 (18)	7 (23)
Sierra de Urbasa (9)	7 (39)	3 (35)	8 (39)	23 (37)	14 (39)	5 (39)	11 (40)	30 (40)
Cuenca de Pamplona (10)	8 (39)	4 (35)	6 (34)	23 (35)	12 (34)	5 (31)	7 (35)	36 (37)
Peña Izaga y Lumbier (11)	7 (40)	2 (34)	3 (39)	17 (39)	14 (32)	12 (29)	13 (39)	31 (40)
Valles bajos Roncal y Salazar (12)	6 (40)	2 (40)	10 (40)	32 (40)	9 (40)	5 (40)	9 (40)	26 (40)
Tierra Estella Norte (13)	4 (18)	5 (14)	13 (19)	23 (19)	9 (18)	15 (18)	26 (18)	7 (19)
Entorno Puente la Reina (14)	5 (39)	3 (26)	18 (40)	17 (40)	6 (31)	8 (40)	13 (40)	31 (40)
Macizo zona media (15)	4 (39)	4 (39)	26 (39)	9 (37)	13 (35)	12 (35)	24 (40)	9 (40)
Sierra Peña de Leire (16)	1 (29)	6 (19)	13 (19)	9 (23)	15 (19)	21 (19)	31 (27)	4 (35)
Tierra Estella sur (17)	3 (35)	15 (39)	15 (23)	10 (27)	7 (19)	17 (34)	23 (34)	9 (31)
Ribera Alta (18)	3 (19)	2 (24)	16 (39)	27 (39)	3 (31)	2 (35)	6 (39)	41 (40)
Bardenas Reales (19)	4 (40)	14 (37)	15 (37)	12 (37)	8 (39)	7 (39)	24 (39)	16 (40)
Ribera Baja (20)	6 (19)	14 (35)	16 (40)	8 (39)	5 (40)	4 (40)	27 (40)	21 (40)

Fuel moisture scenarios were derived for each pyrome from the distribution of the Energy Release Component for fuel model G (ERC-G). For the 70th, 85th, and 97th ERC-G percentiles, Fire Family Plus was applied to the weather records from the selected automatic weather stations (Table A2) to estimate dead and live fuel moisture values. The resulting percentile-specific inputs are reported in Table A4.

Table A4. Pyrome-specific fuel moisture contents (%) for the 70th, 85th, and 97th ERC-G percentile scenarios. Values are reported for 1, 10, and 100 h dead fuels and for live herbaceous and live woody fuels. Pyromes 4 and 8 inherited the wind and fuel moisture scenarios from their assigned neighboring pyrome 7, as indicated in Table A2.

Pyrome (Code)	1 h	10 h	100 h	Herbaceous	Woody	ERC-G Perc.
Bidasoa (1)	6.8	7.1	8	22.9	72.3	97
	8.7	8.8	9.8	32.8	76.5	85
	10.5	10.6	11.3	32.8	78.1	70
Urumea (2)	9.1	9.7	11.9	20.5	76.5	97
	12.1	12.5	14.9	32.2	85.7	85
	16.2	16.5	18.1	47.6	93.4	70

Table A4. *Cont.*

Pyrome (Code)	1 h	10 h	100 h	Herbaceous	Woody	ERC-G Perc.
Ulzama (3)	6.9	7.1	8.4	6.9	60	97
	9.3	9.6	11	9.3	60	85
	11	11	11.9	11	60	70
Irati-Alduides (4), inherited from 7	7	7.2	8.1	7	60	97
	9.5	9.7	11	9.5	60	85
	11.7	12	13.1	11.7	60	70
Barranca (5)	6	6.3	7.5	6	67.7	97
	8.4	8.6	9.3	8.5	75.5	85
	6	6.3	7.5	6	67.7	70
Itoiz y Valle Erro Medio (6)	6.3	6.4	7.1	6.3	60.2	97
	8.9	8.9	9.2	9.5	66.8	85
	10.8	10.8	11.3	13.1	81.2	70
Alto Valle Salazar y Lintzoain (7)	7	7.2	8.1	7	60	97
	9.5	9.7	11	9.5	60	85
	11.7	12	13.1	11.7	60	70
Norte Valle del Roncal (8), inherited from 7	7	7.2	8.1	7	60	97
	9.5	9.7	11	9.5	60	85
	11.7	12	13.1	11.7	60	70
Sierra de Urbasa (9)	6.2	6.7	8.7	6.2	84.4	97
	8.7	8.9	10.2	8.7	95	85
	11	11.1	11.7	13.1	102.6	70
Cuenca de Pamplona (10)	4.2	4.5	5.7	4.2	60.1	97
	5.5	5.8	6.9	5.5	61.9	85
	7.1	7.2	7.6	7.1	64.1	70
Peña Izaga y Lumbier (11)	3.8	4	5.1	3.8	60	97
	5.1	5.2	6.1	5.1	60	85
	5.6	5.7	6.3	5.6	60	70
Valles bajos Roncal y Salazar (12)	7.3	7.5	8.2	7.3	60	97
	9.9	10.3	12.3	9.9	60	85
	13.2	13.3	14.8	13.2	60	70
Tierra Estella Norte (13)	4.5	4.8	5.8	4.5	60	97
	5.6	5.9	6.7	5.6	60.1	85
	6.4	6.5	7.1	6.4	60.7	70
Entorno Puente La Reina (14)	4.8	5.1	6.1	4.8	60.5	97
	6.8	7	7.6	7.7	66.9	85
	8.1	8.3	8.9	11.4	72.8	70
Macizo zona media (15)	4	4.2	5.2	4	60	97
	5.3	5.4	6.1	5.3	60.2	85
	6.5	6.5	6.9	6.5	61.2	70
Sierra Peña de Leire (16)	4.3	4.5	5.2	4.3	60	97
	5	5.2	6	5	60	85
	5.7	5.8	6.4	5.7	60.1	70
Tierra Estella sur (17)	4.8	5	5.6	4.8	59.5	97
	5.5	5.6	6.2	5.5	65.5	85
	6.1	6.2	6.9	6.1	68.5	70

Table A4. *Cont.*

Pyrome (Code)	1 h	10 h	100 h	Herbaceous	Woody	ERC-G Perc.
Ribera Alta (18)	4.4	4.6	5.5	4.4	60	97
	5.4	5.5	6.1	5.4	60	85
	6.1	6.1	6.6	6.1	60	70
Bardenas Reales (19)	2.9	3.1	3.8	2.9	54.3	97
	4.9	5	5.5	4.9	60	85
	5.2	5.3	5.9	5.2	65.8	70
Ribera Baja (20)	5	5.2	5.9	5	62.5	97
	6	6.2	6.8	6	67.5	85
	7	7	7.5	7.1	71.7	70

Appendix B. Assignment of Standard Fuel Models to Vegetation Types

The assignment of standard fuel models used in this study reflects the variability in vegetation types across the study area (Table A5). Shrub strata were classified as low shrub ($h < 0.75$ m), medium shrub ($0.75 \leq h < 1.5$ m), and tall shrub ($1.5 \leq h < 3$ m). Forest classes were differentiated into coniferous and broadleaved types and further subdivided according to understory height, including forests with low understory ($h < 0.75$ m), medium understory ($0.75 \leq h < 1.5$ m), and tall understory ($1.5 \leq h < 3$ m). This classification was based on the 2016 PNOA LiDAR flight and required an accumulation of at least 75% of LiDAR returns within the defined height ranges. The 2016 PNOA LiDAR flight for Navarra was acquired between September and November 2017 using a Leica SPL100 sensor (a Leica SPL100 sensor (Leica Geosystems AG, Heerbrugg, Switzerland)), with a point density of 14 points m^{-2}, horizontal and vertical accuracies of 0.20 m and 0.15 m RMSE, respectively, and simultaneous acquisition of RGB and infrared imagery [56]. A canopy cover greater than 15% was used as the threshold to identify forest fuels. Additional masks were used to delineate herbaceous fuel models, including rainfed cereal fields and grasslands, and non-burnable areas, including rivers, rocky outcrops, irrigated land, and intensively tilled cropland, using SIGPAC 2024 [89]. Three climate zones were considered in the fuel model assignment: humid (H), Mediterranean (M), and semi-arid (S).

Table A5. Assignment table of Scott and Burgan (2005) standard fuel models to vegetation types.

Code	Fuel Model	Climate	Disturbance	Vegetation Type
20	108	H	na	Rainfed crops
21	103	H	na	Rainfed woody crops
22	105	H	na	Grasslands and pastures
24	146	H	unburned and low severity	Low shrubland (<0.75 m)
25	148	H	unburned and low severity	Medium shrubland (0.75–1.5 m)
26	149	H	unburned and low severity	Tall shrubland (1.5–3 m)
27	144	H	unburned and low severity	Conifer forest with low shrub understory
28	143	H	unburned and low severity	Conifer forest with medium shrub understory
29	203	H	unburned and low severity	Conifer forest with tall shrub understory
31	162	H	unburned and low severity	Broadleaf forest with medium shrub understory
32	163	H	unburned and low severity	Broadleaf forest with tall shrub understory

Table A5. *Cont.*

Code	Fuel Model	Climate	Disturbance	Vegetation Type
124	105	H	moderate severity	Low shrubland (<0.75 m)
125	105	H	moderate severity	Medium shrubland (0.75–1.5 m)
126	143	H	moderate severity	Tall shrubland (1.5–3 m)
127	105	H	moderate severity	Conifer forest with low shrub understory
128	183	H	moderate severity	Conifer forest with medium shrub understory
129	183	H	moderate severity	Conifer forest with tall shrub understory
131	182	H	moderate severity	Broadleaf forest with medium shrub understory
132	186	H	moderate severity	Broadleaf forest with tall shrub understory
1024	103	H	high severity	Low shrubland (<0.75 m)
1025	105	H	high severity	Medium shrubland (0.75–1.5 m)
1026	143	H	high severity	Tall shrubland (1.5–3 m)
1027	103	H	high severity	Conifer forest with low shrub understory
1028	181	H	high severity	Conifer forest with medium shrub understory
1029	181	H	high severity	Conifer forest with tall shrub understory
1031	182	H	high severity	Broadleaf forest with medium shrub understory
1032	182	H	high severity	Broadleaf forest with tall shrub understory
20	107	M	na	Rainfed crops
21	102	M	na	Rainfed woody crops
22	104	M	na	Grasslands and pastures
24	121	M	unburned and low severity	Low shrubland (<0.75 m)
25	122	M	unburned and low severity	Medium shrubland (0.75–1.5 m)
26	123	M	unburned and low severity	Tall shrubland (1.5–3 m)
27	183	M	unburned and low severity	Conifer forest with low shrub understory
28	188	M	unburned and low severity	Conifer forest with medium shrub understory
29	165	M	unburned and low severity	Conifer forest with tall shrub understory
31	189	M	unburned and low severity	Broadleaf forest with medium shrub understory
32	147	M	unburned and low severity	Broadleaf forest with tall shrub understory
124	102	M	moderate severity	Low shrubland (<0.75 m)
125	121	M	moderate severity	Medium shrubland (0.75–1.5 m)
126	122	M	moderate severity	Tall shrubland (1.5–3 m)
127	102	M	moderate severity	Conifer forest with low shrub understory
128	181	M	moderate severity	Conifer forest with medium shrub understory
129	183	M	moderate severity	Conifer forest with tall shrub understory
131	182	M	moderate severity	Broadleaf forest with medium shrub understory
132	186	M	moderate severity	Broadleaf forest with tall shrub understory
1024	101	M	high severity	Low shrubland (<0.75 m)
1025	102	M	high severity	Medium shrubland (0.75–1.5 m)
1026	121	M	high severity	Tall shrubland (1.5–3 m)
1027	101	M	high severity	Conifer forest with low shrub understory

Table A5. *Cont.*

Code	Fuel Model	Climate	Disturbance	Vegetation Type
1028	102	M	high severity	Conifer forest with medium shrub understory
1029	102	M	high severity	Conifer forest with tall shrub understory
1031	182	M	high severity	Broadleaf forest with medium shrub understory
1032	182	M	high severity	Broadleaf forest with tall shrub understory
20	102	S	na	Rainfed crops
21	93	S	na	Rainfed woody crops
22	101	S	na	Grasslands and pastures
24	141	S	unburned and low severity	Low shrubland (<0.75 m)
25	142	S	unburned and low severity	Medium shrubland (0.75–1.5 m)
26	145	S	unburned and low severity	Tall shrubland (1.5–3 m)
27	183	S	unburned and low severity	Conifer forest with low shrub understory
28	161	S	unburned and low severity	Conifer forest with medium shrub understory
29	165	S	unburned and low severity	Conifer forest with tall shrub understory
31	189	S	unburned and low severity	Broadleaf forest with medium shrub understory
32	147	S	unburned and low severity	Broadleaf forest with tall shrub understory
124	101	S	moderate severity	Low shrubland (<0.75 m)
125	121	S	moderate severity	Medium shrubland (0.75–1.5 m)
126	141	S	moderate severity	Tall shrubland (1.5–3 m)
127	102	S	moderate severity	Conifer forest with low shrub understory
128	181	S	moderate severity	Conifer forest with medium shrub understory
129	183	S	moderate severity	Conifer forest with tall shrub understory
131	182	S	moderate severity	Broadleaf forest with medium shrub understory
132	182	S	moderate severity	Broadleaf forest with tall shrub understory
1024	101	S	high severity	Low shrubland (<0.75 m)
1025	102	S	high severity	Medium shrubland (0.75–1.5 m)
1026	121	S	high severity	Tall shrubland (1.5–3 m)
1027	101	S	high severity	Conifer forest with low shrub understory
1028	102	S	high severity	Conifer forest with medium shrub understory
1029	102	S	high severity	Conifer forest with tall shrub understory
1031	182	S	high severity	Broadleaf forest with medium shrub understory
1032	182	S	high severity	Broadleaf forest with tall shrub understory

Appendix C. Applicability Assessment of the Ignition Probability Model

The stochastic simulations used an ignition probability (IP) grid derived from a logit fire occurrence model previously developed for central Navarra [51]. Because that model was calibrated within a smaller central Navarra frame, we evaluated its applicability before using it across the full regional modeling domain. The IP grid was used as a relative spatial weighting surface for sampling ignition locations in the simulations.

The original occurrence model was based mainly on anthropogenic predictors, including distance to settlements, roads, railways, and power lines, population density, and land use. This is consistent with the predominantly human-caused ignition regime in Navarra.

To assess transferability, we extracted predicted IP values for two independent observed ignition datasets: (i) ignitions recorded after the original calibration period, from 2014 to 2024, and (ii) ignitions recorded up to 2013 but located outside of the original calibration frame. These observed points were compared with a random background sample distributed across the analysis domain.

We evaluated model discrimination using presence background AUC, with observed ignitions treated as presences and random points as background points. In this context, AUC represents the probability that a randomly selected ignition point has a higher predicted IP value than a randomly selected background point. We also compared observed and random IP distributions using the Mann–Whitney U test and assessed ignition concentration in the highest-ranked portions of the IP surface. AUC confidence intervals were estimated through non-parametric bootstrap resampling.

Observed ignitions were consistently associated with higher predicted IP values than random background points (Figure A2a). The median IP value was 0.731 for the 2014–2024 temporal holdout and 0.728 for the pre-2013 outside-frame spatial holdout, compared with 0.675 for random background points. AUC values were similar for both independent evaluations, 0.622 and 0.621, respectively, and the combined observed dataset produced an AUC of 0.622 (Table A6; Figure A2b). Mann–Whitney tests confirmed that observed ignitions had significantly higher IP values than random points. The highest 30% of the background IP distribution contained 47.4% of post-2014 ignitions and 48.2% of pre-2013 outside-frame ignitions, while the highest 50% contained approximately 69% of ignitions in both datasets.

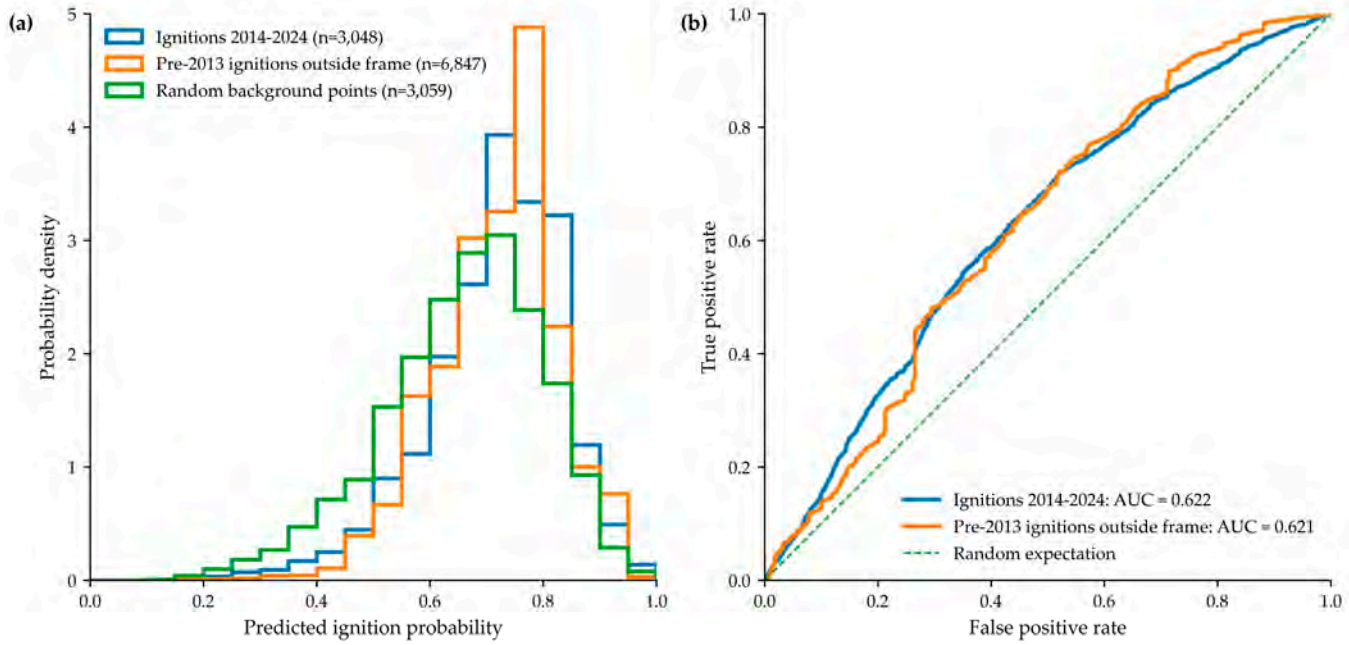

Figure A2. External applicability assessment of the ignition probability (IP) surface. Distribution of predicted IP values extracted at post-2014 observed ignitions, pre-2013 ignitions outside of the original calibration frame, and random background points (**a**). Presence-background receiver operating characteristic curves comparing observed ignition datasets with random background points. The AUC values indicate modest but consistent rank discrimination, supporting use of the IP surface as a relative ignition sampling grid for regional stochastic simulations (**b**).

Table A6. External assessment of the ignition probability (IP) surface used for stochastic ignition placement. Observed ignitions were compared with random background points. The 2014–2024 dataset provides a temporal holdout, the pre-2013 outside-frame dataset provides a spatial transfer test, and the combined dataset summarizes the overall external check. The column n indicates the number of observed ignition points in each evaluation dataset. AUC values indicate presence-background rank discrimination and are followed by 95% bootstrap confidence intervals.

Evaluation Dataset	Ignition Points (n)	Median IP	Random Median IP	AUC vs. Random
Ignitions 2014–2024	3048	0.731	0.675	0.622, 95% CI 0.611–0.636
Ignitions $\leq$ 2013 outside of calibration frame	6847	0.728	0.675	0.621, 95% CI 0.610–0.635
Both observed datasets combined	9895	0.729	0.675	0.622, 95% CI 0.611–0.634

These results indicate that the transferred IP grid retained useful regional rank discrimination. The AUC values were lower than those reported for the original model calibration, as expected when applying a model outside of its calibration frame and across a larger, more heterogeneous region. Nevertheless, the consistency between temporal and spatial holdout tests supports using the IP surface as a practical relative ignition sampling grid. Remaining uncertainty is acknowledged for pyromes where local ignition processes differ from the anthropogenic gradients represented by the model.

Appendix D. Fire Spread Model Calibration and Annualization

Fire spread model calibration and annualization were conducted independently for 10 macroareas or pyroregions, each composed of one or several neighboring pyromes with similar landscape fuels, topography, observed fire size distributions, and mean annual burned area (Figure A1; Table A7). Simulations were run separately within each macroarea. The number of modeled years and simulated ignitions varied among macroareas to obtain spatially continuous and stable burn probability surfaces. Therefore, unequal simulation numbers were used to improve Monte Carlo convergence and were not used as weights when merging the regional outputs. Larger simulation libraries were required in low-frequency mountainous and eastern macroareas, where historical fires rarely exceeded 100 ha, because repeated sampling was needed to stabilize burn probabilities across the landscape.

Ignition locations were sampled within each macroarea using the ignition probability grid. For each simulated fire, fuel moisture conditions were randomly assigned from the pyrome-specific ERC-G percentile scenarios reported in Table A4 using 60% of fires under the 97th percentile, 30% under the 85th percentile, and 10% under the 70th percentile. Wind direction was sampled from the observed wildfire season frequency distribution for each pyrome during the 10:00–18:00 active spread period, whereas wind speed was represented by the corresponding 97th percentile value for each direction. This design was intended to represent the active spread conditions associated with large fire growth in Navarra rather than the full distribution of daily fire weather conditions. Fire spread duration was calibrated by macroarea using the combinations shown in Table A7. These duration mixtures were selected to reproduce the observed fire size distribution and historical mean annual burned area in each macroarea.

Table A7. Fire spread calibration and simulation design by macroarea. Fire spread modeling was conducted independently for 10 macroareas or pyroregions. Historical burned area corresponds to the mean annual burned area calculated from 38 years of fire records and was used as the macroarea-specific annualization target. The number of modeled years and simulated ignitions varied among macroareas to obtain stable burn probability surfaces, while fire spread duration mixtures were calibrated to reproduce observed fire size distributions.

Macroarea	Pyromes	Historical Burned Area (ha yr^{-1})	Fire Ignitions (no.)	Modeled Years (no.)	Fire Spread Duration (% Ignitions and min)
1	1	398	78,955	50,000	60 min (70%), 90 min (17%), 120 min (5%), 210 min (8%)
2	2, 3	65	131,707	50,000	90 min (100%)
3	4, 6, 7	52	265,181	75,000	60 min (100%)
4	8, 12	9	209,501	150,000	60 min (100%)
5	5, 9, 13	55	247,188	200,000	30 min (100%)
6	10, 11	132	37,909	50,000	30 min (75%), 60 min (15%), 90 min (10%)
7	14, 15, 16	679	82,639	50,000	30 min (88%), 240 min (12%)
8	17, 18	147	65,794	100,000	30 min (85%), 60 min (15%)
9	19	109	48,287	100,000	30 min (65%), 60 min (35%)
10	20	31	173,272	50,000	30 min (100%)

For calibration, observed and simulated fires were assigned to the macroarea where the ignition point was located. Observed and modeled fire size distributions were then compared by macroarea using fixed fire size classes (Figure A3). Macroareas with multi-class large fire distributions showed close agreement between observed and modeled fire size frequencies. Macroareas not shown in Figure A3 had observed and modeled fires concentrated in the smallest fire size class, from 0.1 to 0.2 thousand ha.

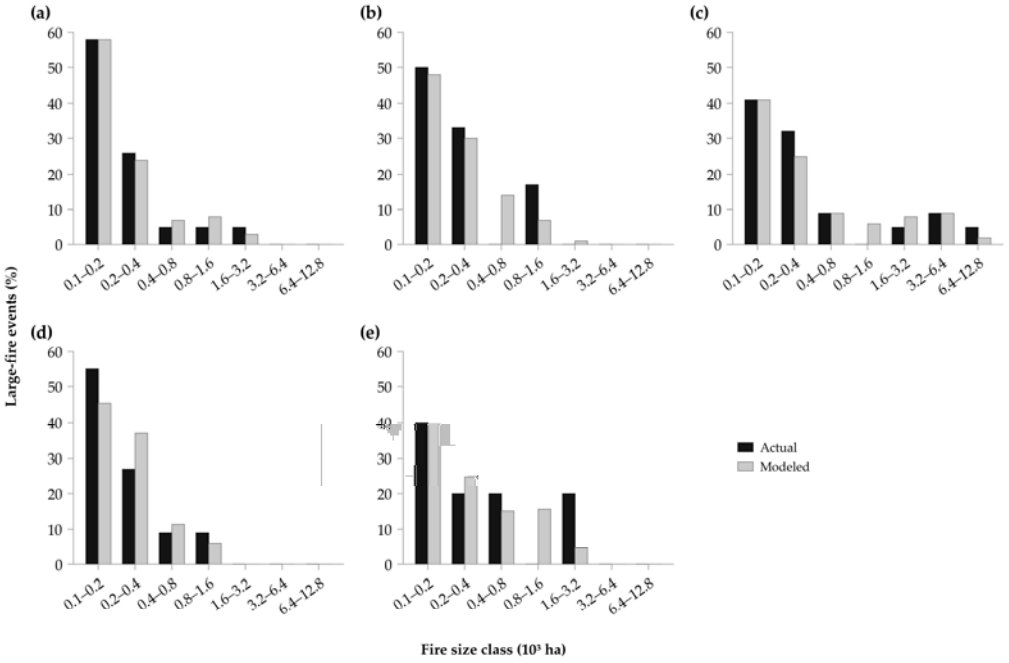

Figure A3. Observed and modeled fire size distributions for Macroarea 1 (**a**), Macroarea 6 (**b**), Macroarea 7 (**c**), Macroarea 8 (**d**), and Macroarea 9 (**e**). Fire size classes are expressed in thousand ha. Macroareas not shown had observed and modeled fires concentrated in the smallest fire size class, from 0.1 to 0.2 thousand ha.

Annualization was performed within each macroarea before assembling the regional products. The historical mean annual burned area calculated from 38 years of fire records (1985 to 2022) was used as the macroarea-specific annualization target (Table A7), and fire spread durations were adjusted so that simulated fire size distributions reproduced the observed burned area regime. For each macroarea, burn probability was calculated using the macroarea-specific number of modeled years as the denominator, rather than pooling simulations across macroareas under a common denominator. Exposure metrics were calculated analogously by averaging burned area, burned forest area, and exposed structures over the modeled years within each macroarea. The final regional layers and summary tables were then produced by mosaicking or summing these macroarea-specific annualized outputs. Thus, macroareas with larger simulation libraries contributed according to their calibrated annual fire occurrence and burned area regime, not according to the raw number of simulated ignitions.

Appendix E. Community Exposure to Wildfires

Table A8. Community-level wildfire exposure across municipalities and supramunicipal units in Navarra. Values include population, mean annual burned area in cropland, pasture, shrubland, tall shrubland and young woodland, and forest land, together with the mean annual number of exposed residential buildings and industrial structures, total structure counts, and unit area. Abbreviations: aBA = mean annual burned area; aBFA = mean annual burned forest area.

Code	Municipality	Area (ha)	Residential Buildings (no.)	Industrial Structures (no.)	Exposed Residential Buildings (no. year^{-1})	Exposed Industrial Structures (no. year^{-1})	aBFA (ha year^{-1})
1	Abáigar	495	120	7	0.029	0.011	0.052
2	Abárzuza/Abartzuza	1466	362	34	0.224	0.073	0.379
3	Abaurregaina/Abaurrea Alta	2090	199	12	0.334	0.035	0.796
4	Abaurrepea/Abaurrea Baja	1111	69	7	0.061	0.008	0.382
5	Aberin	2113	343	10	0.441	0.019	0.561
6	Ablitas	7741	2172	84	0.221	0.020	0.202
7	Adiós	835	143	4	0.873	0.031	0.524
8	Aguilar de Codés	1862	212	74	0.051	0.008	0.106
9	Aibar/Oibar	4795	848	127	0.795	0.169	1.025
10	Altsasu/Alsasua	2680	1660	203	0.030	0.004	0.045
11	Allín/Allin	4300	1025	91	0.572	0.069	0.732
12	Allo	3626	1029	49	0.649	0.063	0.328
13	Améscoa Baja	4683	855	80	0.120	0.020	0.372
14	Ancín/Antzin	880	329	18	0.018	0.003	0.110
15	Andosilla	5151	1836	114	0.193	0.038	0.165
16	Ansoáin/Antsoain	191	318	116	0.022	0.002	0.019
17	Anue	6150	496	65	0.322	0.045	1.914
18	Añorbe	2409	415	48	1.193	0.260	1.220
19	Aoiz/Agoitz	1313	762	69	0.130	0.007	0.219
20	Araitz	3943	535	69	0.263	0.032	1.155
21	Aranarache/Aranaratxe	507	69	20	0.005	0.002	0.019
22	Arantza	3024	684	13	0.231	0.004	0.760
23	Aranguren	4054	2387	906	1.429	0.123	1.288
24	Arano	1330	196	7	0.071	0.001	0.282
25	Arakil	5251	888	122	0.147	0.027	0.249

Table A8. *Cont.*

Code	Municipality	Area (ha)	Residential Buildings (no.)	Industrial Structures (no.)	Exposed Residential Buildings (no. year^{-1})	Exposed Industrial Structures (no. year^{-1})	aBFA (ha year^{-1})
26	Aras	1790	279	28	0.034	0.005	0.100
27	Arbizu	1431	743	70	0.067	0.006	0.042
28	Arce/Artzi	14,636	430	18	0.188	0.008	3.120
29	Los Arcos	5719	1006	88	0.153	0.044	0.173
30	Arellano	1680	259	4	0.191	0.008	0.170
31	Areso	1202	252	51	0.115	0.022	0.390
32	Arguedas	6642	1724	114	0.192	0.041	0.277
33	Aria	818	83	6	0.051	0.004	0.348
34	Aribe	432	63	2	0.015	0.000	0.126
35	Armañanzas	1227	180	11	0.091	0.006	0.076
36	Arróniz	5519	932	50	0.284	0.038	0.284
37	Arruazu	573	114	6	0.006	0.001	0.019
38	Artajona	6690	1414	201	1.656	0.630	2.216
39	Artazu	599	121	12	0.352	0.035	0.353
40	Atetz	2665	371	45	0.568	0.080	1.151
41	Ayegui/Aiegi	958	1764	24	0.338	0.005	0.241
42	Azagra	3329	1750	53	0.083	0.006	0.039
43	Azuelo	1106	121	22	0.023	0.001	0.061
44	Bakaiku	1170	211	16	0.010	0.001	0.027
45	Barásoain	1405	379	90	0.834	0.373	0.724
46	Barbarin	844	83	3	0.058	0.003	0.013
47	Bargota	2545	409	21	0.090	0.008	0.142
48	Barillas	295	303	0	0.030	0.000	0.001
49	Basaburua	8231	824	108	1.098	0.153	4.863
50	Baztan	37,092	6582	402	4.630	0.304	14.608
51	Beire	2237	479	35	0.915	0.114	0.072
52	Belascoáin	607	168	34	0.191	0.049	0.337
53	Berbinzana	1313	647	40	0.187	0.018	0.218
54	Bertizarana	3875	608	25	0.313	0.012	1.238
55	Betelu	687	188	14	0.031	0.002	0.202
56	Biurrun-Olcoz	1657	277	26	1.346	0.197	1.597
57	Buñuel	3616	1731	279	0.121	0.019	0.020
58	Auritz/Burguete	1923	264	16	0.232	0.021	0.441
59	Burgui/Burgi	6458	352	21	0.015	0.002	0.159
60	Burlada/Burlata	215	812	60	0.009	0.001	0.001
61	El Busto	735	125	2	0.115	0.003	0.020
62	Cabanillas	3574	1172	156	0.203	0.218	0.336
63	Cabredo	1200	180	7	0.000	0.000	0.010
64	Cadreita	2731	1440	145	0.084	0.048	0.033
65	Caparroso	8068	1925	534	0.401	0.309	1.275
66	Cárcar	4023	1035	89	0.139	0.046	0.078
67	Carcastillo	9728	2212	192	0.349	0.085	0.586
68	Cascante	6315	2747	155	0.299	0.045	0.097
69	Cáseda	8527	1055	155	0.798	0.109	2.308
70	Castejón	1845	2005	145	0.062	0.006	0.021

Table A8. *Cont.*

Code	Municipality	Area (ha)	Residential Buildings (no.)	Industrial Structures (no.)	Exposed Residential Buildings (no. year^{-1})	Exposed Industrial Structures (no. year^{-1})	aBFA (ha year^{-1})
71	Castillonuevo/Gazteluberri	2671	71	0	0.016	0.000	0.143
72	Cintruénigo	3734	4135	414	0.171	0.044	0.057
73	Ziordia	1439	292	23	0.013	0.002	0.022
74	Cirauqui/Zirauki	4137	473	12	1.420	0.051	4.122
75	Ciriza/Ziritza	369	225	13	0.426	0.026	0.164
76	Cizur	4647	1402	123	3.967	0.503	2.187
77	Corella	8107	3858	213	0.431	0.037	0.058
78	Cortes	3669	2243	151	0.044	0.011	0.009
79	Desojo	1412	194	17	0.159	0.018	0.135
80	Dicastillo	3332	606	32	0.255	0.039	0.330
81	Donamaria	2383	505	15	0.538	0.016	0.919
82	Etxalar	4705	897	49	0.236	0.016	1.201
83	Echarri/Etxarri	220	168	8	0.449	0.023	0.092
84	Etxarri Aranatz	3302	931	117	0.063	0.016	0.085
85	Etxauri	1364	400	22	0.396	0.041	0.483
86	Valle de Egüés/Eguesibar	5350	2377	116	0.964	0.098	1.118
87	Elgorriaga	391	216	6	0.111	0.004	0.166
88	Valle de Elorz/Elortzibar	4829	1763	652	1.066	0.101	1.044
89	Enériz/Eneritz	945	314	10	1.017	0.047	0.828
90	Eratsun	2613	256	8	0.104	0.002	1.121
91	Ergoiena	4180	453	21	0.078	0.005	0.203
92	Erro	14,428	1116	54	0.446	0.027	3.062
93	Ezcároz/Ezkaroze	2927	286	18	0.066	0.005	0.329
94	Eslava	1926	236	5	0.821	0.021	1.093
95	Esparza de Salazar	2692	125	2	0.009	0.000	0.263
96	Espronceda	876	191	18	0.060	0.010	0.117
97	Estella-Lizarra	1539	2544	160	0.712	0.058	0.453
98	Esteribar	14,915	2013	203	0.784	0.081	4.073
99	Etayo	1320	104	5	0.129	0.018	0.256
100	Eulate	1038	284	7	0.043	0.002	0.046
101	Ezcabarte	3405	1078	202	0.841	0.094	1.162
102	Ezkurra	2382	257	27	0.094	0.009	1.116
103	Ezprogui	4655	141	13	0.252	0.032	0.861
104	Falces	11,500	1610	144	0.226	0.168	0.295
105	Fitero	4323	1715	82	0.174	0.027	0.364
106	Fontellas	2204	864	39	0.082	0.007	0.057
107	Funes	5268	1305	270	0.049	0.038	0.111
108	Fustiñana	6714	1874	173	0.221	0.122	0.310
109	Galar	4475	1219	477	2.519	0.176	2.550
110	Gallipienzo/Galipentzu	5629	408	12	0.949	0.041	3.578
111	Gallués/Galoze	4341	204	22	0.043	0.005	0.433
112	Garaioa	2117	131	20	0.217	0.029	0.805
113	Garde	4342	203	18	0.004	0.000	0.053
114	Garínoain	1026	336	35	0.555	0.198	0.707
115	Garralda	2124	227	16	0.122	0.014	0.767

Table A8. *Cont.*

Code	Municipality	Area (ha)	Residential Buildings (no.)	Industrial Structures (no.)	Exposed Residential Buildings (no. year^{-1})	Exposed Industrial Structures (no. year^{-1})	aBFA (ha year^{-1})
116	Genevilla	873	195	27	0.000	0.000	0.001
117	Goizueta	9135	785	23	0.567	0.011	4.145
118	Goñi	4223	300	21	0.278	0.017	0.915
119	Güesa/Gorza	2684	110	4	0.027	0.001	0.179
120	Guesálaz/Gesalatz	7682	1019	23	2.178	0.053	3.554
121	Guirguillano	2460	190	11	0.504	0.035	1.354
122	Huarte/Uharte	382	959	280	0.037	0.016	0.008
123	Uharte Arakil	3794	504	96	0.043	0.011	0.170
124	Ibargoiti	5405	342	79	0.199	0.031	0.873
125	Igúzquiza	1802	372	7	0.137	0.007	0.279
126	Imotz	4240	534	73	0.428	0.063	1.362
127	Irañeta	840	163	18	0.015	0.003	0.026
128	Isaba/Izaba	14,741	532	23	0.020	0.001	0.349
129	Ituren	1501	594	30	0.352	0.012	0.653
130	Iturmendi	991	250	46	0.022	0.006	0.021
131	Iza/Itza	5203	992	65	0.954	0.080	1.118
132	Izagaondoa	5961	327	19	0.326	0.018	1.045
133	Izalzu/Itzaltzu	730	72	11	0.007	0.001	0.092
134	Jaurrieta	3098	248	9	0.126	0.008	0.794
135	Javier	4652	144	4	0.100	0.006	1.816
136	Juslapeña/Txulapain	3163	516	44	0.778	0.084	1.274
137	Beintza-Labaien	2798	502	36	0.316	0.022	1.383
138	Lakuntza	1103	556	122	0.028	0.006	0.033
139	Lana	4998	399	10	0.050	0.002	0.327
140	Lantz	1694	174	18	0.333	0.029	1.095
141	Lapoblación	1800	323	28	0.024	0.003	0.027
142	Larraga	7720	1488	109	0.705	0.195	1.765
143	Larraona	1043	170	6	0.011	0.001	0.030
144	Larraun	10,777	1027	189	1.067	0.276	3.420
145	Lazagurría	1658	265	17	0.074	0.008	0.117
146	Leache/Leatxe	1476	120	4	0.140	0.007	0.272
147	Legarda	845	127	5	0.665	0.028	0.524
148	Legaria	499	180	35	0.014	0.002	0.017
149	Leitza	5833	1199	166	0.751	0.124	2.869
150	Leoz/Leotz	9622	513	172	2.094	0.581	13.026
151	Lerga	2131	205	22	0.654	0.100	1.802
152	Lerín	9797	1573	101	0.625	0.117	1.555
153	Lesaka	5520	1375	108	0.180	0.009	0.495
154	Lezaun	1943	293	52	0.109	0.021	0.352
155	Liédena	1902	358	14	0.137	0.011	0.234
156	Lizoain-Arriasgoiti	6524	496	17	0.486	0.023	1.167
157	Lodosa	4567	2328	188	0.561	0.036	0.299
158	Lónguida/Longida	9072	529	24	0.300	0.017	1.159
159	Lumbier	5690	913	126	0.255	0.084	0.703
160	Luquin	879	159	0	0.047	0.000	0.022

Table A8. *Cont.*

Code	Municipality	Area (ha)	Residential Buildings (no.)	Industrial Structures (no.)	Exposed Residential Buildings (no. year^{-1})	Exposed Industrial Structures (no. year^{-1})	aBFA (ha year^{-1})
161	Mañeru	1289	359	19	0.794	0.047	0.781
162	Marañón	687	142	37	0.000	0.000	0.009
163	Marcilla	2170	1406	155	0.066	0.022	0.112
164	Mélida	2608	1127	61	0.160	0.025	0.312
165	Mendavia	7796	2573	145	0.083	0.023	0.296
166	Mendaza	3277	820	58	0.387	0.030	0.315
167	Mendigorria	3930	1029	70	2.238	0.264	1.414
168	Metauten	2216	338	67	0.273	0.098	0.244
169	Milagro	2854	2206	153	0.047	0.036	0.050
170	Mirafuentes	280	117	15	0.037	0.008	0.034
171	Miranda de Arga	6012	878	27	0.213	0.020	0.268
172	Monreal/Elo	2250	354	23	0.143	0.015	0.622
173	Monteagudo	1091	902	25	0.084	0.003	0.007
174	Morentin	894	193	5	0.205	0.007	0.167
175	Mues	1439	199	11	0.029	0.008	0.120
176	Murchante	1338	2453	387	0.238	0.094	0.024
177	Murieta	442	365	44	0.019	0.011	0.038
178	Murillo el Cuende	5938	839	152	0.493	0.139	0.476
179	Murillo el Fruto	3340	836	47	1.220	0.096	1.437
180	Muruzábal	627	294	10	0.661	0.021	0.187
181	Navascués/Nabaskoze	9602	407	23	0.133	0.015	1.106
182	Nazar	643	109	6	0.090	0.007	0.093
183	Obanos	1974	712	32	0.814	0.117	0.542
184	Oco	337	73	1	0.122	0.001	0.012
185	Ochagavía/Otsagabia	11,503	516	31	0.095	0.017	1.398
186	Odieta	2400	427	60	0.521	0.086	0.876
187	Oiz	800	183	4	0.122	0.002	0.289
188	Oláibar	1572	332	26	0.253	0.027	0.594
189	Olazti/Olazagutía	1962	610	97	0.021	0.004	0.037
190	Olejua	441	55	4	0.105	0.013	0.075
191	Olite/Erriberri	8403	2395	138	0.634	0.111	0.257
192	Olóriz/Oloritz	4008	292	69	1.185	0.169	3.891
193	Cendea de Olza/Oltza Zendea	4067	1302	173	2.053	0.161	1.519
194	Valle de Ollo/Ollaran	3698	516	26	0.288	0.015	0.858
195	Orbaizeta	8231	280	15	0.137	0.004	1.338
196	Orbara	914	80	3	0.033	0.002	0.376
197	Orísoain	711	107	6	0.685	0.038	1.079
198	Oronz/Orontze	1110	74	0	0.011	0.000	0.092
199	Oroz-Betelu/Orotz-Betelu	2346	239	20	0.155	0.028	0.877
200	Oteiza	4802	775	30	2.042	0.249	1.960
201	Pamplona/Iruña	2509	8377	438	0.295	0.077	0.038
202	Peralta/Azkoien	8836	2313	701	0.154	0.135	0.502
203	Petilla de Aragón	2798	98	26	0.001	0.000	0.019
204	Piedramillera	1125	162	7	0.324	0.023	0.158
205	Pitillas	4234	691	31	0.507	0.121	0.355

Table A8. *Cont.*

Code	Municipality	Area (ha)	Residential Buildings (no.)	Industrial Structures (no.)	Exposed Residential Buildings (no. year^{-1})	Exposed Industrial Structures (no. year^{-1})	aBFA (ha year^{-1})
206	Puente la Reina/Gares	3969	1127	133	1.293	0.171	1.522
207	Pueyo/Puiu	2122	550	37	1.833	0.201	1.720
208	Ribaforada	2902	2450	162	0.100	0.016	0.020
209	Romanzado/Erromantzatua	9169	373	20	0.341	0.021	1.283
210	Roncal/Erronkari	3883	248	36	0.005	0.001	0.098
211	Orreaga/Roncesvalles	1509	44	7	0.018	0.005	0.262
212	Sada	1267	271	4	0.338	0.010	0.318
213	Saldias	900	224	7	0.151	0.007	0.233
214	Salinas de Oro/Jaitz	1428	161	37	0.131	0.032	0.820
215	San Adrián	2106	2261	162	0.073	0.010	0.100
216	Sangüesa/Zangoza	6834	2609	322	1.241	0.252	0.956
217	San Martín de Unx	5014	655	43	2.846	0.234	3.145
219	Sansol	1331	148	4	0.086	0.005	0.056
220	Santacara	3427	1017	42	1.395	0.139	0.974
221	Doneztebe/Santesteban	860	610	60	0.174	0.018	0.297
222	Sarriés/Sartze	2314	101	4	0.025	0.001	0.173
223	Sartaguda	1487	1163	115	0.042	0.026	0.030
224	Sesma	7122	1076	133	0.251	0.163	0.509
225	Sorlada	641	138	13	0.239	0.029	0.088
226	Sunbilla	1033	723	20	0.182	0.005	0.248
227	Tafalla	9829	2959	372	3.141	0.630	2.261
228	Tiebas-Muruarte de Reta	2170	615	57	1.554	0.091	0.970
229	Tirapu	562	82	18	0.510	0.142	0.459
230	Torralba del Río	1769	257	32	0.047	0.008	0.152
231	Torres del Río	1281	277	5	0.099	0.001	0.060
232	Tudela	21,568	7776	944	0.892	0.203	1.104
233	Tulebras	382	331	6	0.044	0.002	0.004
234	Úcar	1186	186	11	1.023	0.057	1.157
235	Ujué/Uxue	11,188	583	66	3.197	0.402	19.204
236	Ultzama	9657	1364	170	3.207	0.449	5.350
237	Unciti	3734	288	9	0.414	0.015	0.732
238	Unzué/Untzue	1855	162	39	0.498	0.102	1.930
239	Urdazubi/Urdax	754	429	19	0.232	0.010	0.219
240	Urdiain	1508	459	50	0.040	0.005	0.034
241	Urraúl Alto	14,159	416	26	0.459	0.037	2.833
242	Urraúl Bajo	5942	387	41	0.261	0.030	0.699
243	Urroz-Villa	1142	300	25	0.168	0.021	0.089
244	Urroz	1046	259	16	0.152	0.011	0.332
245	Urzainqui/Urzainki	2061	103	2	0.001	0.000	0.062
246	Uterga	923	201	5	0.871	0.013	0.616
247	Uztárroz/Uztarroze	5819	216	2	0.006	0.000	0.236
248	Luzaide/Valcarlos	4466	554	8	0.131	0.003	0.912
249	Valtierra	4985	1601	164	0.119	0.034	0.388
250	Bera	3542	1442	71	0.180	0.004	0.343
251	Viana	7848	1622	242	0.099	0.023	0.102

Table A8. *Cont.*

Code	Municipality	Area (ha)	Residential Buildings (no.)	Industrial Structures (no.)	Exposed Residential Buildings (no. year^{-1})	Exposed Industrial Structures (no. year^{-1})	aBFA (ha year^{-1})
252	Vidángoz/Bidankoze	3922	127	5	0.005	0.000	0.135
253	Bidaurreta	509	140	13	0.203	0.022	0.438
254	Villafranca	4680	1648	218	0.113	0.064	0.155
255	Villamayor de Monjardín	1314	118	3	0.036	0.001	0.140
256	Hiriberri/Villanueva de Aezkoa	2131	164	4	0.222	0.003	0.945
257	Villatuerta	2359	687	103	0.745	0.148	1.598
258	Villava/Atarrabia	108	546	54	0.045	0.005	0.002
259	Igantzi	1663	515	8	0.185	0.003	0.292
260	Valle de Yerri/Deierri	9345	1879	140	4.659	0.374	3.937
261	Yesa	2222	433	26	0.091	0.009	0.222
262	Zabalza/Zabaltza	1415	230	24	0.787	0.069	0.737
263	Zubieta	1806	459	18	0.167	0.006	0.619
264	Zugarramurdi	565	275	14	0.103	0.005	0.170
265	Zúñiga	1186	191	19	0.024	0.005	0.065
901	Barañáin/Barañain	139	371	42	0.014	0.000	0.002
902	Berrioplano/Berriobeiti	2574	1426	641	0.764	0.189	0.474
903	Berriozar	269	638	134	0.063	0.011	0.047
904	Irurtzun	352	398	52	0.008	0.001	0.022
905	Beriáin	542	693	175	1.138	0.091	0.068
906	Orkoien	562	851	259	0.187	0.017	0.054
907	Zizur Mayor/Zizur Nagusia	511	1518	14	0.657	0.004	0.022
908	Lekunberri	662	619	87	0.051	0.014	0.110

Appendix F. Protected Area Exposure to Wildfires

This appendix summarizes modeled wildfire exposure for each protected area in Navarra, including total and forested burned area for all fires, medium- and high-intensity fires, and high-intensity fires only.

Table A9. Protected area exposure to wildfire in Navarra. Values include total protected area extent, mean annual burned area, mean annual burned area at flame lengths greater than 1.5 m and 2.5 m, and the corresponding metrics for forested land only. Abbreviations: aBA = mean annual burned area; aBFA = mean annual burned forest area; SNR = Strict Nature Reserve; NP = Natural Park; NR = Nature Reserve; NE = Natural Enclave; PL = Protected Landscape; RNA = Recreational Natural Area; and PPZ = Peripheral Protection Zone.

Code	Protected Area	Type	IUCN Cat.	Area (ha)	aBA (ha year^{-1})	aBA$^{1.5}$ (ha year^{-1})	aBA$^{2.5}$ (ha year^{-1})	aBFA (ha year^{-1})	aBFA$^{1.5}$ (ha year^{-1})	aBFA$^{2.5}$ (ha year^{-1})
ANR 1	Bosque de Orgi	RNA	VI	80.9	0.037	0.012	0.004	0.034	0.011	0.003
ANR 2	Embalses de Leurza	RNA	VI	365.9	0.138	0.054	0.012	0.093	0.02	0.002
EN 1	Hayedo de Odia	NE	IV	43.1	0.01	0.002	0	0.01	0.002	0
EN 1	Hayedo de Odia	PPZ	VI	72.9	0.033	0.021	0.005	0.016	0.006	0.001
EN 2	Foz de Ugarrón	NE	IV	98.6	0.08	0.077	0.063	0.037	0.035	0.031
EN 2	Foz de Ugarrón	PPZ	VI	97	0.087	0.078	0.054	0.044	0.036	0.025

Table A9. *Cont.*

Code	Protected Area	Type	IUCN Cat.	Area (ha)	aBA (ha year^{-1})	aBA$^{1.5}$ (ha year^{-1})	aBA$^{2.5}$ (ha year^{-1})	aBFA (ha year^{-1})	aBFA$^{1.5}$ (ha year^{-1})	aBFA$^{2.5}$ (ha year^{-1})
EN 3	Pinares de Lerin	NE	IV	97.3	0.201	0.18	0.138	0.145	0.131	0.1
EN 3	Pinares de Lerin	PPZ	VI	192	0.56	0.538	0.481	0.057	0.053	0.044
EN 4	Pinar de Santa Agueda	NE	IV	65	0.051	0.045	0.036	0.034	0.03	0.023
EN 4	Pinar de Santa Agueda	PPZ	VI	137	0.126	0.106	0.097	0.01	0.01	0.008
EN 5	Soto de Campo Allende	NE	IV	11.1	0.014	0.013	0.009	0.012	0.011	0.008
EN 5	Soto de Campo Allende	PPZ	VI	8	0.011	0.002	0.001	0.003	0.001	0.001
EN 6	Sotos Lopez-Val	NE	IV	17.8	0.013	0.002	0.001	0.011	0.001	0
EN 6	Sotos Lopez-Val	PPZ	VI	33.5	0.014	0.01	0.006	0.012	0.008	0.005
EN 7	Sotos de la Recueja	NE	IV	56.1	0.027	0.016	0.007	0.024	0.014	0.006
EN 7	Sotos de la Recueja	PPZ	VI	42.8	0.027	0.019	0.014	0.01	0.009	0.007
EN 8	Badina Escudera	NE	IV	27.2	0.003	0.001	0.001	0	0	0
EN 8	Badina Escudera	PPZ	VI	63.8	0.018	0.005	0.004	0	0	0
EN 9	Soto de Granjafría	NE	IV	36.5	0.003	0.002	0.001	0.002	0.002	0.001
EN 9	Soto de Granjafría	PPZ	VI	13.5	0.001	0.001	0	0	0	0
EN 10	Sotos de Murillos de las Limas	NE	IV	110.8	0.015	0.01	0.006	0.011	0.008	0.004
EN 10	Sotos de Murillos de las Limas	PPZ	VI	73.3	0.013	0.006	0.004	0.003	0.002	0.001
EN 11	Sotos de Traslapuente	NE	IV	40.7	0.006	0.003	0.002	0.005	0.003	0.002
EN 11	Sotos de Traslapuente	PPZ	VI	2.8	0	0	0	0	0	0
EN 12	Soto de la Mejana de Santa Isabel	NE	IV	17.7	0.001	0	0	0.001	0	0
EN 12	Soto de la Mejana de Santa Isabel	PPZ	VI	18.8	0.002	0	0	0	0	0
EN 13	Laguna de Dos Reinos	NE	IV	32.2	0.001	0.001	0.001	0	0	0
EN 13	Laguna de Dos Reinos	PPZ	VI	11.6	0.001	0	0	0	0	0
EN 14	Soto de Campollano	NE	IV	10.9	0.007	0.004	0.002	0.006	0.003	0.002
EN 14	Soto de Campollano	PPZ	VI	0.3	0	0	0	0	0	0
EN 15	Soto de la Biona	NE	IV	3.3	0.003	0.002	0	0.002	0.001	0
EN 15	Soto de la Biona	PPZ	VI	20.2	0.014	0.012	0.004	0.006	0.005	0.002
EN 16	Soto de Escueral	NE	IV	14.3	0.028	0.015	0.007	0.023	0.013	0.006
EN 16	Soto de Escueral	PPZ	VI	17.6	0.037	0.033	0.021	0.023	0.02	0.012
EN 17	Soto Sequedo	NE	IV	20.3	0.006	0.002	0	0.005	0.001	0
EN 17	Soto Sequedo	PPZ	VI	18.4	0.005	0.003	0.001	0.003	0.002	0.001
EN 18	Soto Artica	NE	IV	11.6	0.011	0.007	0.004	0.01	0.007	0.004
EN 19	Soto Arenales	NE	IV	24.1	0.038	0.032	0.021	0.035	0.029	0.02
EN 19	Soto Arenales	PPZ	VI	12.4	0.025	0.02	0.015	0.023	0.018	0.014
EN 20	Soto Valporres-Soto Abajo	NE	IV	35.5	0.058	0.031	0.016	0.048	0.023	0.011
EN 20	Soto Valporres-Soto Abajo	PPZ	VI	6.8	0.013	0.006	0.003	0.008	0.003	0.002
EN 21	Sotos de Rada	NE	IV	27.8	0.029	0.026	0.02	0.022	0.019	0.014
EN 21	Sotos de Rada	PPZ	VI	4.4	0.005	0.003	0.002	0.002	0.002	0
EN 22	Sotos de la Muga	NE	IV	37	0.003	0.001	0.001	0.001	0	0
EN 22	Sotos de la Muga	PPZ	VI	3.3	0	0	0	0	0	0
EN 23	Soto de Santa Eulalia	NE	IV	7.5	0.001	0	0	0	0	0
EN 23	Soto de Santa Eulalia	PPZ	VI	27.2	0.003	0.001	0.001	0	0	0
EN 24	Soto Alto	NE	IV	10.1	0.002	0.001	0.001	0.001	0.001	0
EN 24	Soto Alto	PPZ	VI	13.5	0.003	0.002	0.001	0.002	0.001	0.001
EN 25	Soto Giraldelli	NE	IV	17.4	0.002	0.001	0.001	0	0	0
EN 25	Soto Giraldelli	PPZ	VI	21.3	0.005	0.004	0.003	0.002	0.001	0.001
EN 26	Soto de la Mora	NE	IV	11.8	0.001	0	0	0.001	0	0
EN 26	Soto de la Mora	PPZ	VI	7.1	0.001	0	0	0	0	0

Table A9. *Cont.*

Code	Protected Area	Type	IUCN Cat.	Area (ha)	aBA (ha year^{-1})	aBA$^{1.5}$ (ha year^{-1})	aBA$^{2.5}$ (ha year^{-1})	aBFA (ha year^{-1})	aBFA$^{1.5}$ (ha year^{-1})	aBFA$^{2.5}$ (ha year^{-1})
EN 27	Encinares de Betelu	NE	IV	52.4	0.025	0.012	0.003	0.025	0.012	0.003
EN 28	Soto de los Tetones	NE	IV	113.1	0.022	0.002	0.001	0.001	0	0
PN 1	Señorío de Bertiz	NP	II	2052.3	0.423	0.026	0	0.416	0.024	0
PN 2	Sierras de Urbasa y Andía	NP	V	20941.7	5.164	4.724	3.54	0.961	0.682	0.465
PN 3	Bardenas Reales	NP	II	41517.6	49.914	48.623	45.167	0.807	0.773	0.671
PP 1	Montes de la Valdorba	PL	V	3389.6	16.229	14.895	12.053	7.37	6.789	5.662
PP 2	Robledales de Ultzama y Basaburua	PL	V	8237.5	12.265	7.826	3.606	4.924	1.821	0.459
PP 3	Concejo de Elia	PL	V	524.7	0.255	0.157	0.065	0.223	0.133	0.053
PP 4	Señorio de Egulbati	PL	V	264.2	0.111	0.065	0.025	0.089	0.047	0.017
RI 1	Lizardoya	SNR	Ib	64	0.007	0.001	0	0.007	0.001	0
RI 2	Ukerdi	SNR	Ib	313.6	0.005	0.002	0.001	0.005	0.002	0
RI 3	Aztaparreta	SNR	Ib	175.4	0.003	0	0	0.003	0	0
RI 3	Aztaparreta	PPZ	VI	165.3	0.008	0.006	0.002	0.003	0.001	0
RN 1	Labiaga	RN	IV	1.4	0	0	0	0	0	0
RN 2	Itxusi	RN	IV	115.6	0.12	0.098	0.031	0.053	0.043	0.013
RN 2	Itxusi	PPZ	VI	76.6	0.045	0.03	0.007	0.032	0.021	0.005
RN 3	San Juan Xar	RN	IV	2.7	0	0	0	0	0	0
RN 3	San Juan Xar	PPZ	VI	8.7	0.003	0.001	0	0.002	0.001	0
RN 4	Irubetakaskoa	RN	IV	116.3	0.026	0.008	0.001	0.025	0.007	0.001
RN 4	Irubetakaskoa	PPZ	VI	89.4	0.033	0.016	0.003	0.03	0.013	0.002
RN 5	Cueva Basajaun-Etxea de Lanz	RN	IV	0	0	0	0	0	0	0
RN 6	Mendilaz	RN	IV	139.6	0.027	0.014	0.006	0.02	0.007	0.002
RN 6	Mendilaz	PPZ	VI	193	0.123	0.103	0.049	0.013	0.005	0.001
RN 7	Putxerri	RN	IV	82.4	0.007	0	0	0.007	0	0
RN 7	Putxerri	PPZ	VI	68.3	0.006	0	0	0.006	0	0
RN 8	Tristuibartea	RN	IV	56.5	0.012	0.002	0.001	0.012	0.002	0
RN 8	Tristuibartea	PPZ	VI	40.5	0.018	0.01	0.004	0.012	0.005	0.001
RN 9	Foz de Iñarbe	RN	IV	276.5	0.074	0.045	0.011	0.073	0.045	0.011
RN 9	Foz de Iñarbe	PPZ	VI	151.8	0.051	0.031	0.01	0.049	0.03	0.01
RN 10	Poche de Txintxurrenea	RN	IV	37.9	0.008	0.006	0.002	0.008	0.006	0.002
RN 10	Poche de Txintxurrenea	PPZ	VI	50.5	0.021	0.014	0.008	0.014	0.009	0.003
RN 11	Gaztelu	RN	IV	76.8	0.024	0.013	0.003	0.022	0.012	0.003
RN 11	Gaztelu	PPZ	VI	91.9	0.036	0.022	0.008	0.033	0.02	0.006
RN 12	Larra	RN	IV	2731.2	0.025	0.01	0.003	0.021	0.008	0.002
RN 12	Larra	PPZ	VI	495.2	0.036	0.029	0.012	0.01	0.007	0.003
RN 13	Barranco de Lasia	RN	IV	21.6	0.001	0.001	0	0.001	0.001	0
RN 13	Barranco de Lasia	PPZ	VI	22.8	0.002	0.002	0.001	0.002	0.002	0.001
RN 14	Nacedero del Urederra	RN	IV	111.2	0.007	0.004	0.001	0.006	0.003	0.001
RN 14	Nacedero del Urederra	PPZ	VI	56.2	0.006	0.005	0.003	0.003	0.003	0.002
RN 15	Basau	RN	IV	84.3	0.006	0.003	0.001	0.006	0.003	0.001
RN 15	Basaura	PPZ	VI	111.9	0.014	0.011	0.006	0.014	0.011	0.006
RN 16	Foz de Arbayun	RN	IV	1178.3	0.24	0.194	0.129	0.206	0.164	0.112
RN 17	Foz de Benasa	RN	IV	160.5	0.011	0.006	0.001	0.011	0.006	0.001
RN 17	Foz de Benasa	PPZ	VI	83	0.007	0.003	0.001	0.006	0.003	0.001
RN 18	Foz de Burgui	RN	IV	197.3	0.01	0.007	0.003	0.009	0.007	0.003
RN 18	Foz de Burgui	PPZ	VI	46.4	0.003	0.002	0	0.003	0.002	0

Table A9. *Cont.*

Code	Protected Area	Type	IUCN Cat.	Area (ha)	aBA (ha year^{-1})	aBA$^{1.5}$ (ha year^{-1})	aBA$^{2.5}$ (ha year^{-1})	aBFA (ha year^{-1})	aBFA$^{1.5}$ (ha year^{-1})	aBFA$^{2.5}$ (ha year^{-1})
RN 19	Peñalabeja	RN	IV	23.3	0	0	0	0	0	0
RN 19	Peñalabeja	PPZ	VI	67.5	0	0	0	0	0	0
RN 20	Embalse de Salobre o de las Cañas	RN	IV	100.3	0.015	0.011	0.004	0	0	0
RN 20	Embalse de Salobre o de las Cañas	PPZ	VI	92.3	0.021	0.019	0.014	0.001	0.001	0.001
RN 21	Monte de Olleta	RN	IV	27.5	0.083	0.081	0.072	0.082	0.08	0.071
RN 21	Monte de Olleta	PPZ	VI	93	0.266	0.256	0.224	0.215	0.207	0.183
RN 22	Monte del Conde	RN	IV	136.3	0.627	0.616	0.577	0.612	0.601	0.565
RN 22	Monte del Conde	PPZ	VI	159.4	0.786	0.629	0.471	0.266	0.247	0.208
RN 23	Laguna del Juncal	RN	IV	9.7	0.018	0.016	0.01	0	0	0
RN 23	Laguna del Juncal	PPZ	VI	34.2	0.072	0.069	0.062	0	0	0
RN 24	Acantilados de la Piedra y San Adrián	RN	IV	289.6	0.126	0.111	0.073	0.069	0.062	0.042
RN 24	Acantilados de la Piedra y San Adrián	PPZ	VI	146.2	0.08	0.066	0.039	0.027	0.022	0.014
RN 25	Foz de Lumbier	RN	IV	44.8	0.008	0.007	0.003	0.004	0.003	0.002
RN 25	Foz de Lumbier	PPZ	VI	82.3	0.023	0.017	0.008	0.007	0.006	0.004
RN 26	Caparreta	RN	IV	34.8	0.025	0.019	0.011	0.022	0.018	0.011
RN 26	Caparreta	PPZ	VI	124.8	0.073	0.042	0.021	0.067	0.038	0.019
RN 27	Laguna de Pitillas	RN	IV	215.5	0.643	0.517	0.266	0.002	0.002	0.001
RN 27	Laguna de Pitillas	PPZ	VI	197.8	1.598	1.409	0.959	0.048	0.044	0.033
RN 28	Sotos del Arquillo y Barbaraces	RN	IV	27.3	0.008	0.007	0.006	0.002	0.002	0.002
RN 28	Sotos del Arquillo y Barbaraces	PPZ	VI	56.9	0.019	0.013	0.008	0.002	0.002	0.001
RN 29	Sotos de La Lobera y El Sotillo	RN	IV	64.8	0.04	0.035	0.028	0.022	0.02	0.016
RN 29	Sotos de La Lobera y El Sotillo	PPZ	VI	131.8	0.141	0.106	0.083	0.043	0.039	0.031
RN 30	Sotos Gil y Ramal Hondo	RN	IV	52.8	0.006	0.004	0.003	0.003	0.002	0.002
RN 30	Sotos Gil y Ramal Hondo	PPZ	VI	32.1	0.003	0	0	0	0	0
RN 31	Vedado de Egüaras	RN	IV	501.5	0.649	0.626	0.578	0.102	0.097	0.088
RN 31	Vedado de Egüaras	PPZ	VI	246.5	0.389	0.386	0.366	0.014	0.014	0.012
RN 32	Soto del Ramalete	RN	IV	48.7	0.003	0.001	0	0.003	0	0
RN 32	Soto del Ramalete	PPZ	VI	40.5	0.006	0.001	0.001	0.001	0	0
RN 33	Sotos de la Remonta	RN	IV	44.1	0.004	0.001	0.001	0.003	0.001	0.001
RN 33	Sotos de la Remonta	PPZ	VI	46.8	0.007	0.001	0.001	0	0	0
RN 34	Balsa de Agua Salada	RN	IV	16.3	0.009	0.009	0.008	0	0	0
RN 34	Balsa de Agua Salada	PPZ	VI	35.7	0.023	0.022	0.021	0	0	0
RN 35	Balsa del Pulguer	RN	IV	48.6	0.039	0.038	0.033	0.001	0.001	0.001
RN 35	Balsa del Pulguer	PPZ	VI	47.1	0.102	0.097	0.088	0.001	0.001	0.001
RN 36	Rincon del Bu	RN	IV	464.8	0.449	0.446	0.392	0.008	0.008	0.007
RN 36	Rincon del Bu	PPZ	VI	257.2	0.272	0.272	0.254	0.001	0.001	0
RN 37	Caídas de la Negra	RN	IV	1457.4	0.495	0.465	0.387	0.249	0.226	0.185
RN 37	Caídas de la Negra	PPZ	VI	658.7	0.34	0.337	0.311	0.053	0.052	0.046
RN 38	Soto del Quebrado, El Ramillo y La Mejana	RN	IV	47.4	0.006	0.004	0.002	0.004	0.003	0.002
RN 38	Soto del Quebrado, El Ramillo y La Mejana	PPZ	VI	17.5	0.003	0.001	0.001	0	0	0

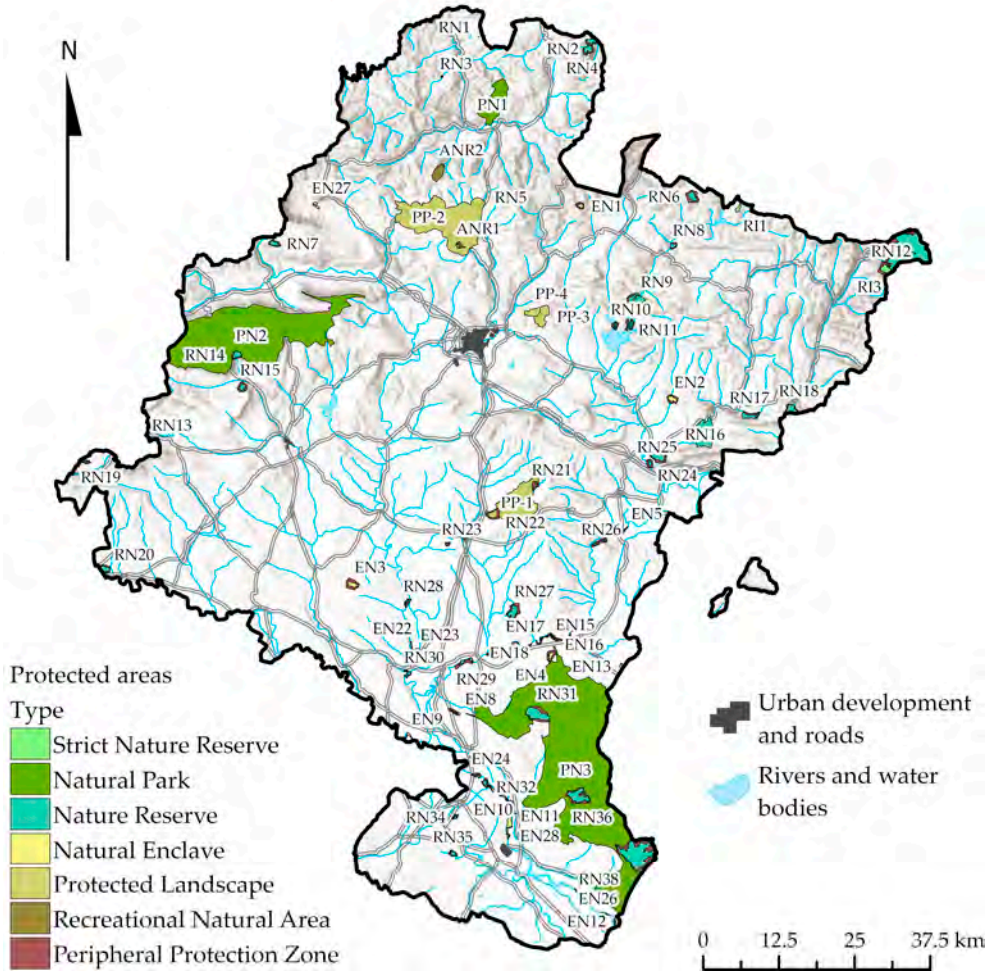

Figure A4. Protected areas in Navarra colored by protected area type. Table A9 provides the correspondence between protected area abbreviations and exposure results. Note that some protected areas include a Peripheral Protection Zone, which is represented separately from the core protected area.

References

1. Benali, A.; Guiomar, N.; Gonçalves, H.; Mota, B.; Silva, F.; Fernandes, P.M.; Mota, C.; Penha, A.; Santos, J.; Pereira, J.M.C.; et al. The Portuguese Large Wildfire Spread Database (PT-FireSprd). *Earth Syst. Sci. Data* **2023**, *15*, 3791–3818. [CrossRef]
2. Chas-Amil, M.-L.; García-Martínez, E.; Touza, J. Iberian Peninsula October 2017 Wildfires: Burned Area and Population Exposure in Galicia (NW of Spain). *Int. J. Disaster Risk Reduct.* **2020**, *48*, 101623. [CrossRef]
3. Castellnou, M.; Bachfischer, M.; Miralles, M.; Ruiz, B.; Stoof, C.R.; Vilà-Guerau De Arellano, J. Pyroconvection Classification Based on Atmospheric Vertical Profiling Correlation With Extreme Fire Spread Observations. *JGR Atmos.* **2022**, *127*, e2022JD036920. [CrossRef]
4. San-Miguel-Ayanz, J.; Durrant, T.; Boca, R.; Maianti, P.; Liberta, G.; Oom, D.J.F.; Branco, A.; De Rigo, D.; Suarez-Moreno, M.; Ferrari, D.; et al. *Forest Fires in Europe, Middle East and North Africa 2023*; European Union: Luxemburg, 2024; p. 198.
5. San-Miguel-Ayanz, J.; Moreno, J.M.; Camia, A. Analysis of Large Fires in European Mediterranean Landscapes: Lessons Learned and Perspectives. *For. Ecol. Manag.* **2013**, *294*, 11–22. [CrossRef]
6. Moreira, F.; Viedma, O.; Arianoutsou, M.; Curt, T.; Koutsias, N.; Rigolot, E.; Barbati, A.; Corona, P.; Vaz, P.; Xanthopoulos, G.; et al. Landscape–Wildfire Interactions in Southern Europe: Implications for Landscape Management. *J. Environ. Manag.* **2011**, *92*, 2389–2402. [CrossRef]
7. DGPCE. *Informe de Incendios Forestales 2022*; Dirección General de Protección Civil y Emergencias: Madrid, Spain, 2022; p. 39.
8. El Garroussi, S.; Di Giuseppe, F.; Barnard, C.; Wetterhall, F. Europe Faces up to Tenfold Increase in Extreme Fires in a Warming Climate. *npj Clim. Atmos. Sci.* **2024**, *7*, 30. [CrossRef]
9. Jones, M.W.; Abatzoglou, J.T.; Veraverbeke, S.; Andela, N.; Lasslop, G.; Forkel, M.; Smith, A.J.P.; Burton, C.; Betts, R.A.; Van Der Werf, G.R.; et al. Global and Regional Trends and Drivers of Fire Under Climate Change. *Rev. Geophys.* **2022**, *60*, e2020RG000726. [CrossRef]

10. Ellis, T.M.; Bowman, D.M.J.S.; Jain, P.; Flannigan, M.D.; Williamson, G.J. Global Increase in Wildfire Risk Due to Climate-Driven Declines in Fuel Moisture. *Glob. Change Biol.* **2021**, *28*, 1544–1559. [CrossRef] [PubMed]
11. Jain, P.; Castellanos-Acuna, D.; Coogan, S.C.P.; Abatzoglou, J.T.; Flannigan, M.D. Observed Increases in Extreme Fire Weather Driven by Atmospheric Humidity and Temperature. *Nat. Clim. Change* **2022**, *12*, 63–70. [CrossRef]
12. Ameztegui, A.; Morán-Ordóñez, A.; Márquez, A.; Blázquez-Casado, Á.; Pla, M.; Villero, D.; García, M.B.; Errea, M.P.; Coll, L. Forest Expansion in Mountain Protected Areas: Trends and Consequences for the Landscape. *Landsc. Urban Plan.* **2021**, *216*, 104240. [CrossRef]
13. Gelabert, P.J.; Rodrigues, M.; de la Riva, J.; Ameztegui, A.; Sebastià, M.T.; Vega-Garcia, C. LandTrendr Smoothed Spectral Profiles Enhance Woody Encroachment Monitoring. *Remote Sens. Environ.* **2021**, *262*, 112521. [CrossRef]
14. Salis, M.; Del Giudice, L.; Jahdi, R.; Alcasena, F.; Scarpa, C.; Pellizzaro, G.; Bacciu, V.; Schirru, M.; Ventura, A.; Casula, M.; et al. Spatial Patterns and Intensity of Land Abandonment Drive Wildfire Hazard and Likelihood in Mediterranean Agropastoral Areas. *Land* **2022**, *11*, 1942. [CrossRef]
15. Pausas, J.G.; Fernández-Muñoz, S. Fire Regime Changes in the Western Mediterranean Basin: From Fuel-Limited to Drought-Driven Fire Regime. *Clim. Change* **2012**, *110*, 215–226. [CrossRef]
16. Cervera, T.; Pino, J.; Marull, J.; Padró, R.; Tello, E. Understanding the Long-Term Dynamics of Forest Transition: From Deforestation to Afforestation in a Mediterranean Landscape (Catalonia, 1868–2005). *Land Use Policy* **2019**, *80*, 318–331. [CrossRef]
17. Lasanta, T.; Cortijos-López, M.; Errea, M.P.; Khorchani, M.; Nadal-Romero, E. An Environmental Management Experience to Control Wildfires in the Mid-Mountain Mediterranean Area: Shrub Clearing to Generate Mosaic Landscapes. *Land Use Policy* **2022**, *118*, 106147. [CrossRef]
18. Ribeiro, L.M.; Rodrigues, A.; Lucas, D.; Viegas, D.X. The Impact on Structures of the Pedrógão Grande Fire Complex in June 2017 (Portugal). *Fire* **2020**, *3*, 57. [CrossRef]
19. Vacca, P.; Caballero, D.; Pastor, E.; Planas, E. WUI Fire Risk Mitigation in Europe: A Performance-Based Design Approach at Home-Owner Level. *J. Saf. Sci. Resil.* **2020**, *1*, 97–105. [CrossRef]
20. Duane, A.; Moghli, A.; Coll, L.; Vega, C. On the Evidence of Contextually Large Fires in Europe Based on Return Period Functions. *Appl. Geogr.* **2025**, *176*, 103539. [CrossRef]
21. Bacciu, V.; Salis, M.; Arca, B.; Pellizzaro, G.; Ascoli, D.; Delogu, G.; Eftychidis, G.; Chuvieco, E.; Gitas, I.; Viegas, D. Shifting to a Holistic Approach in National Wildfire Management Policies: The Italian Case. *iForest* **2025**, *18*, 163–175. [CrossRef]
22. USDA. *The National Strategy, The Final Phase in the Development of the National Cohesive Wildland Fire Management Strategy*; Forest Service; U.S. Department of Agriculture: Washington, DC, USA, 2014; p. 93.
23. Wunder, S.; Calkin, D.E.; Charlton, V.; Feder, S.; Martínez de Arano, I.; Moore, P.; Rodríguez y Silva, F.; Tacconi, L.; Vega-García, C. Resilient Landscapes to Prevent Catastrophic Forest Fires: Socioeconomic Insights towards a New Paradigm. *For. Policy Econ.* **2021**, *128*, 102458. [CrossRef]
24. Moreira, F.; Ascoli, D.; Safford, H.; Adams, M.A.; Moreno, J.M.; Pereira, J.M.C.; Catry, F.X.; Armesto, J.; Bond, W.; González, M.E.; et al. Wildfire Management in Mediterranean-Type Regions: Paradigm Change Needed. *Environ. Res. Lett.* **2020**, *15*, 011001. [CrossRef]
25. Castellnou, M.; Prat-Guitart, N.; Arilla, E.; Larrañaga, A.; Nebot, E.; Castellarnau, X.; Vendrell, J.; Pallàs, J.; Herrera, J.; Monturiol, M.; et al. Empowering Strategic Decision-Making for Wildfire Management: Avoiding the Fear Trap and Creating a Resilient Landscape. *Fire Ecol.* **2019**, *15*, 31. [CrossRef]
26. Gonzalez-Olabarria, J.R.; Reynolds, K.M.; Larrañaga, A.; Garcia-Gonzalo, J.; Busquets, E.; Pique, M. Strategic and Tactical Planning to Improve Suppression Efforts against Large Forest Fires in the Catalonia Region of Spain. *For. Ecol. Manag.* **2019**, *432*, 612–622. [CrossRef]
27. North, M.P.; Bisbing, S.M.; Hankins, D.L.; Hessburg, P.F.; Hurteau, M.D.; Kobziar, L.N.; Meyer, M.D.; Rhea, A.E.; Stephens, S.L.; Stevens-Rumann, C.S. Strategic Fire Zones Are Essential to Wildfire Risk Reduction in the Western United States. *Fire Ecol.* **2024**, *20*, 50. [CrossRef]
28. Carrasco, J.; Gonzalez-Olabarria, J.R.; Palacios, D.; Mahaluf, R.; Garcia-Gonzalo, J.; Weintraub, A. Multicriteria Firebreak Planning for Protecting Ecological and Cultural Values under Wildfire Risk: A Case Study in Catalonia. *Environ. Sustain. Indic.* **2025**, *28*, 100956. [CrossRef]
29. Oliveira, S.; Gonçalves, A.; Benali, A.; Sá, A.; Zêzere, J.L.; Pereira, J.M. Assessing Risk and Prioritizing Safety Interventions in Human Settlements Affected by Large Wildfires. *Forests* **2020**, *11*, 859. [CrossRef]
30. Thompson, M.; Riley, K.; Loeffler, D.; Haas, J. Modeling Fuel Treatment Leverage: Encounter Rates, Risk Reduction, and Suppression Cost Impacts. *Forests* **2017**, *8*, 469. [CrossRef]
31. Penman, T.D.; Bradstock, R.A.; Price, O.F. Reducing Wildfire Risk to Urban Developments: Simulation of Cost-Effective Fuel Treatment Solutions in South Eastern Australia. *Environ. Model. Softw.* **2014**, *52*, 166–175. [CrossRef]

32. Scott, J.H.; Thompson, M.P.; Gilbertson-Day, J.W. Examining Alternative Fuel Management Strategies and the Relative Contribution of National Forest System Land to Wildfire Risk to Adjacent Homes—A Pilot Assessment on the Sierra National Forest, California, USA. *For. Ecol. Manag.* **2016**, *362*, 29–37. [CrossRef]
33. Parisien, M.-A.; Dawe, D.A.; Miller, C.; Stockdale, C.A.; Armitage, O.B. Applications of Simulation-Based Burn Probability Modelling: A Review. *Int. J. Wildland Fire* **2020**, *28*, 913–926. [CrossRef]
34. Kalabokidis, K.; Palaiologou, P.; Gerasopoulos, E.; Giannakopoulos, C.; Kostopoulou, E.; Zerefos, C. Effect of Climate Change Projections on Forest Fire Behavior and Values-at-Risk in Southwestern Greece. *Forests* **2015**, *6*, 2214–2240. [CrossRef]
35. Lautenberger, C. Mapping Areas at Elevated Risk of Large-Scale Structure Loss Using Monte Carlo Simulation and Wildland Fire Modeling. *Fire Saf. J.* **2017**, *91*, 768–775. [CrossRef]
36. Palaiologou, P.; Kalabokidis, K.; Ager, A.A.; Day, M.A. Development of Comprehensive Fuel Management Strategies for Reducing Wildfire Risk in Greece. *Forests* **2020**, *11*, 789. [CrossRef]
37. Oliveira, S.; Rocha, J.; Sá, A. Wildfire Risk Modeling. *Curr. Opin. Environ. Sci. Health* **2021**, *23*, 100274. [CrossRef]
38. Carlson, A.R.; Hawbaker, T.J.; Bair, L.S.; Hoffman, C.M.; Meldrum, J.R.; Baggett, L.S.; Steblein, P.F. Evaluating a Simulation-Based Wildfire Burn Probability Map for the Conterminous US. *Int. J. Wildland Fire* **2025**, *34*, WF23196. [CrossRef]
39. Haas, J.R.; Calkin, D.E.; Thompson, M.P. A National Approach for Integrating Wildfire Simulation Modeling into Wildland Urban Interface Risk Assessments within the United States. *Landsc. Urban Plan.* **2013**, *119*, 44–53. [CrossRef]
40. Kearns, E.J.; Saah, D.; Levine, C.R.; Lautenberger, C.; Doherty, O.M.; Porter, J.R.; Amodeo, M.; Rudeen, C.; Woodward, K.D.; Johnson, G.W.; et al. The Construction of Probabilistic Wildfire Risk Estimates for Individual Real Estate Parcels for the Contiguous United States. *Fire* **2022**, *5*, 117. [CrossRef]
41. Bar Massada, A.; Syphard, A.D.; Hawbaker, T.J.; Stewart, S.I.; Radeloff, V.C. Effects of Ignition Location Models on the Burn Patterns of Simulated Wildfires. *Environ. Model. Softw.* **2011**, *26*, 583–592. [CrossRef]
42. Finney, M.; McHugh, C.W.; Grenfell, I.C.; Riley, K.L.; Short, K.C. A Simulation of Probabilistic Wildfire Risk Components for the Continental United States. *Stoch. Environ. Res. Risk Assess.* **2011**, *25*, 973–1000. [CrossRef]
43. Aparício, B.A.; Alcasena, F.; Ager, A.; Chung, W.; Pereira, J.M.C.; Sá, A.C.L. Evaluating Priority Locations and Potential Benefits for Building a Nation-Wide Fuel Break Network in Portugal. *J. Environ. Manag.* **2022**, *320*, 115920. [CrossRef] [PubMed]
44. Thompson, M.P.; Vogler, K.C.; Scott, J.H.; Miller, C. Comparing Risk-Based Fuel Treatment Prioritization with Alternative Strategies for Enhancing Protection and Resource Management Objectives. *Fire Ecol.* **2022**, *18*, 26. [CrossRef]
45. Salis, M.; Arca, B.; Del Giudice, L.; Palaiologou, P.; Alcasena, F.; Ager, A.; Fiori, M.; Pellizzaro, G.; Scarpa, C.; Schirru, M.; et al. Application of Simulation Modeling for Wildfire Exposure and Transmission Assessment in Sardinia, Italy. *Int. J. Disaster Risk Reduct.* **2021**, *58*, 102189. [CrossRef]
46. Palaiologou, P.; Ager, A.A.; Nielsen-Pincus, M.; Evers, C.R.; Kalabokidis, K. Using Transboundary Wildfire Exposure Assessments to Improve Fire Management Programs: A Case Study in Greece. *Int. J. Wildland Fire* **2018**, *27*, 501. [CrossRef]
47. Oliveira, S.; Oehler, F.; San-Miguel-Ayanz, J.; Camia, A.; Pereira, J.M.C. Modeling Spatial Patterns of Fire Occurrence in Mediterranean Europe Using Multiple Regression and Random Forest. *For. Ecol. Manag.* **2012**, *275*, 117–129. [CrossRef]
48. Jiménez-Ruano, A.; Mimbrero, M.R.; De La Riva Fernández, J. Understanding Wildfires in Mainland Spain. A Comprehensive Analysis of Fire Regime Features in a Climate-Human Context. *Appl. Geogr.* **2017**, *89*, 100–111. [CrossRef]
49. Gonzalez-Olabarria, J.R.; Mola-Yudego, B.; Pukkala, T.; Palahi, M. Using Multiscale Spatial Analysis to Assess Fire Ignition Density in Catalonia, Spain. *Ann. For. Sci.* **2011**, *68*, 861–871. [CrossRef]
50. Alcasena, F.; Salis, M.; Ager, A.; Castell, R.; Vega-García, C. Assessing Wildland Fire Risk Transmission to Communities in Northern Spain. *Forests* **2017**, *8*, 30. [CrossRef]
51. Alcasena, F.; Salis, M.; Nauslar, N.J.; Aguinaga, A.E.; Vega-García, C. Quantifying Economic Losses from Wildfires in Black Pine Afforestations of Northern Spain. *For. Policy Econ.* **2016**, *73*, 153–167. [CrossRef]
52. Coughlan, M.R. Traditional Fire-Use, Landscape Transition, and the Legacies of Social Theory Past. *Ambio* **2015**, *44*, 705–717. [CrossRef]
53. Jolly, M.; Freeborn, P.H.; Bradshaw, L.S.; Wallace, J.; Brittain, S. Modernizing the US National Fire Danger Rating System (Version 4): Simplified Fuel Models and Improved Live and Dead Fuel Moisture Calculations. *Environ. Model. Softw.* **2024**, *181*, 106181. [CrossRef]
54. Nelson, R.M. A Method for Describing Equilibrium Moisture Content of Forest Fuels. *Can. J. For. Res.* **1984**, *14*, 597–600. [CrossRef]
55. Scott, J.H.; Burgan, R.E. *Standard Fire Behavior Fuel Models: A Comprehensive Set for Use with Rothermel's Surface Fire Spread Model*; USDA Forest Service, Rocky Mountain Research Station: Fort Collins, CO, USA, 2005; p. 72.
56. Instituto Geográfico Nacional; Organismo Autónomo Centro Nacional de Información Geográfica. LiDAR-PNOA 2ª Cobertura (2015–2021): Comunidad Foral de Navarra 2017. Available online: https://centrodedescargas.cnig.es/CentroDescargas/lidar-segunda-cobertura (accessed on 1 January 2024).

57. González-Ferreiro, E.; Diéguez-Aranda, U.; Crecente-Campo, F.; Barreiro-Fernández, L.; Miranda, D.; Castedo-Dorado, F. Modelling Canopy Fuel Variables for Pinus Radiata D. Don in NW Spain with Low-Density LiDAR Data. *Int. J. Wildland Fire* **2014**, *23*, 350–362. [CrossRef]
58. Botequim, B.; Fernandes, P.M.; Borges, J.G.; González-Ferreiro, E.; Guerra-Hernández, J. Improving Silvicultural Practices for Mediterranean Forests through Fire Behaviour Modelling Using LiDAR-Derived Canopy Fuel Characteristics. *Int. J. Wildland Fire* **2019**, *28*, 823–839. [CrossRef]
59. González-Olabarria, J.-R.; Rodríguez, F.; Fernández-Landa, A.; Mola-Yudego, B. Mapping Fire Risk in the Model Forest of Urbión (Spain) Based on Airborne LiDAR Measurements. *For. Ecol. Manag.* **2012**, *282*, 149–156. [CrossRef]
60. Finney, M. Fire Growth Using Minimum Travel Time Methods. *Can. J. For. Res.* **2002**, *32*, 1420–1424. [CrossRef]
61. Brittain, S. Missoula Fire Lab Command Line Applications (unpublished). Available online: https://www.alturassolutions.com/FB/FB_API.htm (accessed on 16 March 2026).
62. Byram, G.M. Forest Fire Behaviour. In *Forest Fire Control and Use*; Davis, K., Ed.; McGraw-Hill: New York, NY, USA, 1959; pp. 90–123.
63. Rothermel, R.C. *A Mathematical Model for Predicting Fire Spread in Wildland Fuels*; USDA Forest Service, Intermountain Forest and Range Experiment Station: Ogden, UT, USA, 1972; p. 40.
64. Palaiologou, P.; Giannakopoulos, C.; Vasilakos, C.; Sakellariou, S.; Rodrigues, M.; Karali, A.; Katavoutas, G.; Varotsos, K.V.; Roussou, O.; Gelabert, P.J.; et al. A Dataset to Support Wildland Fire and Fuel Management in Greece Created with Stochastic Wildfire Simulations. *Data Brief* **2025**, *64*, 112304. [CrossRef]
65. Benali, A.; Benhalima, Y.; Aparício, B.; Timilsina, S.; Keizer, J.; Ager, A. Comparing Pre- and Post-Fire Strategies to Mitigate Wildfire-Induced Soil Erosion in Two Mediterranean Watersheds. *Forests* **2025**, *16*, 1202. [CrossRef]
66. Instituto Geográfico Nacional; Organismo Autónomo Centro Nacional de Información Geográfica. LiDAR-PNOA 3ª Cobertura (2022–2025): Comunidad Foral de Navarra 2024. Available online: https://centrodedescargas.cnig.es/CentroDescargas/lidar-tercera-cobertura (accessed on 16 March 2026).
67. Miller, C.; Ager, A.A. A Review of Recent Advances in Risk Analysis for Wildfire Management. *Int. J. Wildland Fire* **2013**, *22*, 1–14. [CrossRef]
68. Instituto Geográfico Nacional; Centro Nacional de Información Geográfica, O.A. Puntos de interés de la Base Topográfica Nacional (BTN-POI). Edificios 2024. Available online: https://centrodedescargas.cnig.es/CentroDescargas/btn (accessed on 16 March 2026).
69. Aparício, B.A.; Ager, A.A.; Day, M.A. Maximizing Opportunities for Co-Implementing Fuel Break Networks and Restoration Projects. *Front. For. Glob. Change* **2024**, *7*, 1419288. [CrossRef]
70. Teymoor Seydi, S.; Abatzoglou, J.T.; Jones, M.W.; Kolden, C.A.; Filippelli, G.; Hurteau, M.D.; AghaKouchak, A.; Luce, C.H.; Miao, C.; Sadegh, M. Increasing Global Human Exposure to Wildland Fires despite Declining Burned Area. *Science* **2025**, *389*, 826–829. [CrossRef]
71. Ager, A.; Evers, C.; Day, M.; Alcasena, F.; Houtman, R. Planning for Future Fire: Scenario Analysis of an Accelerated Fuel Reduction Plan for the Western United States. *Landsc. Urban Plan.* **2021**, *215*, 104212. [CrossRef]
72. Alcasena, F.; Ager, A.; Belavenutti, P.; Krawchuk, M.; Day, M. Contrasting the Efficiency of Landscape versus Community Protection Fuel Treatment Strategies to Reduce Wildfire Exposure and Risk. *J. Environ. Manag.* **2022**, *309*, 114650. [CrossRef]
73. Jouibary, S.S.; Jahdi, R.; Khalaf, W.A.; Eshaghi, M.A. Burn Probability and Wildfire Risk Modeling of the Protected Areas in Golestan Province, NE Iran. *Geoenviron. Disasters* **2026**, *13*, 32. [CrossRef]
74. Carlson, A.R.; Hawbaker, T.J.; Mockrin, M.H.; Radeloff, V.C.; Bair, L.S.; Caggiano, M.D.; Meldrum, J.R.; Alexandre, P.M.; Kramer, H.A.; Steblein, P.F. Rising Rates of Wildfire Building Destruction in the Conterminous United States. *Proc. Natl. Acad. Sci. USA* **2025**, *122*, e2505886122. [CrossRef]
75. Syphard, A.D.; Rustigian-Romsos, H.; Keeley, J.E. Multiple-Scale Relationships between Vegetation, the Wildland–Urban Interface, and Structure Loss to Wildfire in California. *Fire* **2021**, *4*, 12. [CrossRef]
76. Ager, A.; Day, M.; Alcasena, F.; Evers, C.; Short, K.; Grenfell, I. Predicting Paradise: Modeling Future Wildfire Disasters in the Western US. *Sci. Total Environ.* **2021**, *784*, 147057. [CrossRef]
77. GN. *Plan Especial de Protección Civil de Emergencia Por Incendios Forestales En La Comunidad Foral de Navarra. INFONA 2022*; Departamento de Presidencia, Función Pública, Interior y Justicia: Pamplona, Spain, 2022; p. 162.
78. Fernandes, P.M.; Davies, G.M.; Ascoli, D.; Fernández, C.; Moreira, F.; Rigolot, E.; Stoof, C.R.; Vega, J.A.; Molina, D. Prescribed Burning in Southern Europe: Developing Fire Management in a Dynamic Landscape. *Front. Ecol. Environ.* **2013**, *11*, e4–e14. [CrossRef]
79. Fernandes, P.M.; Vega, J.A.; Jiménez, E.; Rigolot, E. Fire Resistance of European Pines. *For. Ecol. Manag.* **2008**, *256*, 246–255. [CrossRef]
80. Oliveres, J.; Castellnou, M.; Castellarnau, X.; Rosas-Casals, M.; Brotons, L.; Duane, A. The Path to Strategic Fire Management Planning in the Aran, Pyrenees. *Fire Ecol.* **2025**, *21*, 9. [CrossRef]

81. Ascoli, D.; Bovio, G. Prescribed Burning in Italy: Issues, Advances and Challenges. *iForest—Biogeosci. For.* **2013**, *6*, 79–89. [CrossRef]
82. Thompson, M.P.; Calkin, D.E. Uncertainty and Risk in Wildland Fire Management: A Review. *J. Environ. Manag.* **2011**, *92*, 1895–1909. [CrossRef]
83. Riley, K.; Thompson, M. An Uncertainty Analysis of Wildfire Modeling. In *Natural Hazard Uncertainty Assessment: Modeling and Decision Support, Geophysical Monograph 223*; Riley, K., Webley, P., Thompson, M., Eds.; John Wiley & Sons: Hoboken, NJ, USA, 2017; pp. 193–212.
84. Benali, A.; Sa, A.C.; Ervilha, A.R.; Trigo, R.M.; Fernandes, P.M.; Pereira, J.M. Fire Spread Predictions: Sweeping Uncertainty under the Rug. *Sci. Total Environ.* **2017**, *592*, 187–196. [CrossRef] [PubMed]
85. Mauro, F.; Hudak, A.T.; Fekety, P.A.; Frank, B.; Temesgen, H.; Bell, D.M.; Gregory, M.J.; McCarley, T.R. Regional Modeling of Forest Fuels and Structural Attributes Using Airborne Laser Scanning Data in Oregon. *Remote Sens.* **2021**, *13*, 261. [CrossRef]
86. Mauro, F.; Ritchie, M.; Wing, B.; Frank, B.; Monleon, V.; Temesgen, H.; Hudak, A. Estimation of Changes of Forest Structural Attributes at Three Different Spatial Aggregation Levels in Northern California Using Multitemporal LiDAR. *Remote Sens.* **2019**, *11*, 923. [CrossRef]
87. Alcasena, F.; Vega-García, C.; Ager, A.A.; Salis, M.; Nauslar, N.J.; Mendizabal, F.J.; Castell, R. Metodología de evaluación del riesgo de incendios forestales y priorización de tratamientos multifuncionales en paisajes mediterráneos. *CIG* **2019**, *45*, 571–600. [CrossRef]
88. Ager, A.; Aparício, B.A.; Pereira, J.M.C. Optimizing the Portuguese Wildfire Fuel Reduction Program. *Cell Rep. Sustain.* **2025**, *2*, 100361. [CrossRef]
89. Fondo Español de Garantía Agraria (FEGA); Ministerio de Agricultura, Pesca y Alimentación. Recintos del Sistema de Información Geográfica de Parcelas Agrícolas (SIGPAC) 2024. Available online: https://data.europa.eu/data/datasets/spasitnasigpac_pol_recinto_v2024n-xml?locale=en (accessed on 16 March 2026).